HYDRODYNAMICS
CALIFORNIA UNDERSEA AQUEDUCT
APPENDIX III

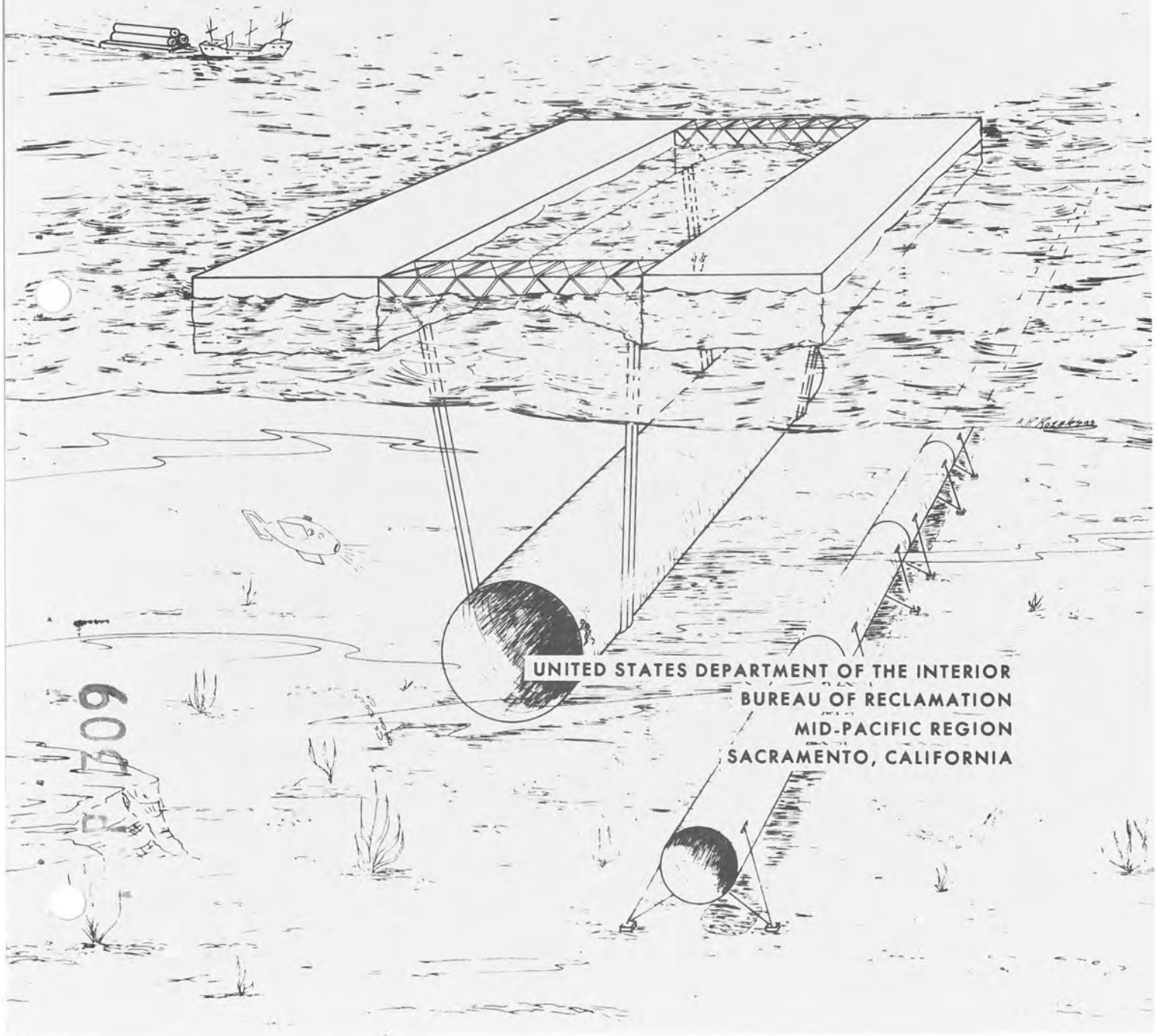

UNITED STATES DEPARTMENT OF THE INTERIOR
BUREAU OF RECLAMATION
MID-PACIFIC REGION
SACRAMENTO, CALIFORNIA

CALIFORNIA UNDERSEA AQUEDUCT RECONNAISSANCE INVESTIGATION

OCEANOGRAPHIC STUDY PROGRAM

APPENDIX III

HYDRODYNAMICS

December 1974

UNITED STATES
DEPARTMENT OF THE INTERIOR

BUREAU OF RECLAMATION

Denver, Colorado

ACKNOWLEDGMENTS

Dr. H. T. Falvey was the hydrodynamics representative for the CUA Management Team from its formation until August 1972. Dr. Falvey, therefore, was the major Bureau contributor in regard to details of understanding with NUC contractors who acquired and analyzed existing data and put them into probabilistic form when possible.

After Mr. Porter's departure, Dr. R. H. Riffenburgh replaced him as principal investigator for the contract work. Dr. Riffenburgh and the staff who worked with him are highly commended for acquiring existing data, determining their quality, and compiling them into more useful forms. Century risk data and construction data for this appendix were extracted from Riffenburgh's work without editing.

A task force group of Bureau personnel compiled a loading and scour data and reference book for use by the Analytical Design Study Task Force. J. C. Schuster collected, analyzed, and wrote the section concerning drag, lift, and mass coefficients. E. R. Ziegler did the portions on general design considerations, buoyancy and wave forces. R. A. Dodge collected material concerning fluid properties and scour.

Especially appreciated were the suggestions for improvements from D. W. Beard, R. B. Hayes, and W. C. Long of the Analytical Design Task Force who selectively used the derived material for the Appraisal Design and Cost Estimates, Appendix I.

CONTENTS

Contents

Contents

FIGURES

Contents

INTRODUCTION

PURPOSE AND SCOPE

This summary contains part of the material generated during the Hydrodynamics Study portion of the Oceanography Study Program. The purpose of the hydrodynamic study was to determine physical properties and variables in the ocean environment and their relationship to the survival of the Aqueduct. Data were to be collected and put into probabilistic form when possible[1]. References concerning data and equations for hydrodynamic loads and scour were to be provided[2]. The style of presentation was not intended for ocean engineering experts but to help Bureau designers to attain sufficient data and knowledge as rapidly as possible in order to make appraisal level "Analytical Design Study" cost estimates. The following criteria guided selection of the contents:

1. Newness of concept or environment and areas of engineering where the USBR has had no or little experience.

2. Technological areas where scale effects or the extreme size of the structure makes interpretation or extrapolation from model studies risky.

3. New compilations and evaluations of existing ocean data, put into probabilistic form when possible.

Design assumptions from the Study Work Plan[3] which also helped to govern the content of this Appendix were that:

1. The Aqueduct would deliver 1 to 4 million acre-feet of water per year.

2. The Aqueduct would include one or more pipes 20 to 32 feet in diameter.

3. The Aqueduct would be located on the Continental Shelf at a depth not exceeding 65 fathoms, or about 400 feet.

4. Design emphasis should be given to the concepts of a buried pipeline, a pipeline partially buried or resting on the bottom, or a flexible buoyant pipeline.

GENERAL CONSIDERATION OF LOADS

Friction and bend head losses are common to all of the pipeline concepts. Water hammer pressure surges in the straight sections, bends, and junctions should be considered by designers. Analysis should be made for each concept. The effects of pipeline orientation, local concentration of head loss and momentum on the motion of the piping system at junctions and couplings should also be considered.

Buried Concept

Buoyant forces acting upon the buried conduit are probably insignificant except for possible soil liquefaction. The buoyant force equation can be used to predict the upward thrust acting on the conduit.

A buried conduit normally is protected from hydrodynamic forces produced by movement of the ocean water. Hydrodynamic forces acting upon the buried conduit would be produced by flow of water within the conduit. Forces occurring at bends should be considered.

Partially Buried or Resting on the Bottom Concept

Buoyant force is present in still or moving water. Buoyant force varies with turbidity, liquefaction of soil, and amount of pipe above the ocean bed.

Introduction

Bend force composed of a static and a dynamic component acts from within the conduit. The static force results from the internal water pressure; the dynamic force is caused by the internal water velocity.

Lift and drag forces occur when the ocean water has a normal component of movement relative to the conduit. Unsteady drag and lift forces can occur because of a periodic vortex formation on the downstream current side of the pipeline.

The conduit can be subject to both steady ocean currents and unsteady velocities caused by wave action. In this case the velocity to be used in the lift and drag force equations is the vector addition of the ocean current velocity and the oscillatory velocity. The dominant source of acceleration is that due to wave action.

Wave action produces an orbiting motion of the water below the water surface. Near the ocean bed, the water oscillates in a general horizontal direction. The velocity periodically increases and decreases and reverses direction to add an acceleration component of unsteadiness to the lift and drag forces. Designers should use appropriate values for lift, drag, and mass coefficients. Values of these coefficients vary, depending on height of pipe above ocean bed, design concept, water velocity, and accelerations caused by currents and waves.

Buoyant Tethered Concept

Normal and parallel hydrodynamic forces act upon the buoyant conduit. Normal forces dominate, but effort should be made to define the parallel forces in relation to the total load on the support and movements of the pipe.

Buoyancy of the conduit is sensitive to the specific weight of fluid surrounding the conduit. Specific weight varies with salinity, and temperature. Specific weight can change in the ocean environment to produce changing loads on the pipe. Density changes and fouling weights should be considered.

A steady ocean current at an angle to the conduit produces two components of force, one normal and one parallel to the conduit. A suction force or negative lift can be caused by proximity to the ocean bottom.

Flowing water in a pipe can produce considerable bend forces that tend to move the conduit and could cause possible "firehose" movement of the Aqueduct.

A tethered buoyant conduit would be more susceptible to ocean wave motion than the other concepts. At a distance above the ocean bed, orbital motion causes horizontal and vertical accelerations and velocities to periodically reverse in direction. Oblique wave crests produce both normal and parallel drag forces on the conduit. When the conduit moves, relative accelerations and velocities between pipe and water should be used in force equations.

FLUID PROPERTIES

GENERAL

Differences of density can be the driving force of ocean currents. For sedimentation and scour, the difference in mass or weight between the seawater and sediment is a driving or a resisting force, depending on whether a particle is settling or resting on the bed.

In hydrodynamics the equation of continuity of flow is derived by accounting for the rate of mass (M) entering and leaving a stationary element of fluid. The equation of motion for the same element can be developed by accounting for the rate of momentum entering, the rate of momentum leaving, and the forces acting on the system. Momentum is the product of velocity (V) and mass (M). Force ($\overline{F}$) is the vector defined in terms of the mass (M) as:

$$\overline{F} = M\overline{a} \tag{1}$$

where ($\overline{a}$) is an acceleration vector. Mass is the measure of the inertia or resistance of a fluid flow to changes of direction and/or velocity. When gravity (g) is considered as the only acceleration acting on the mass, then the force acting in the direction of the gravitational field is called weight (W) expressed as

$$W = Mg \tag{2}$$

Using equations (1) and (2) to solve for (M), equating and then solving for ($\overline{F}$) results in

$$\overline{F} = \frac{W}{g}\overline{a} \tag{2a}$$

where (W/g) is mass expressed in engineering units called slugs.

Fluid Properties

Fluid flow may have a change in mass or weight at different points in the flow system. Thus it is useful to define weight and mass in terms of a unit volume.

$$\gamma = \frac{W}{ft^3}$$

$$\rho = \frac{M}{ft^3} \quad \text{where}$$

W = weight, lbs.

M = mass, slugs, or $\frac{lb\ sec^2}{ft}$

γ = specific weight lb/ft^3

ρ = density, $slugs/ft^3$ or $\frac{lb\ sec^2}{ft^4}$

Using these definitions and substitution into equation (2) results in

$$\gamma = \rho g \qquad (3)$$

Stagnation pressures, drag forces and lift forces are proportional to

$$(\rho V^2),\ \frac{(\gamma V^2)}{g},\ \text{or}\ (MV^2)$$

Mass whether expressed in the form of density or specific weight is a fundamental property in fluid statics and dynamics.

A substance that continues to deform under a sustained shear stress, no matter how small, by definition is a fluid. In real flow, internal shear forces cause heat or frictional losses. If the velocity is great enough, disturbances at boundaries can amplify into general turbulence throughout the entire flow. The property by which a fluid

resists shear is called viscosity. Viscosity can be thought of as the inverse of fluidity.

Viscosity (μ) is defined as the ratio of shearing stress (τ) to the rate of strain. The rate of strain is the velocity gradient (dv/dy). Thus dynamic viscosity is defined as

$$\mu = \frac{\tau}{\frac{dv}{dy}} \tag{4}$$

μ = dynamic viscosity, $\frac{lb/sec}{ft^2}$

τ = shearing stress, lb/ft^2

$\frac{dv}{dy}$ = velocity gradient, $\frac{1}{sec}$

Equation (4) is generally used for steady state flow conditions. However, the kinematic viscosity is used for unsteady flow conditions. Kinematic viscosity (ν) is defined as:

$$\nu = \frac{\mu}{\rho} \tag{5}$$

When hydrodynamic equations of motion are transformed into dimensionless form, both Froude number (N_F) and Reynolds number (N_R) can be formed as coefficients of the dimensionless equation. These numbers are expressed as

$$N_F = \frac{V^2}{Lg}$$

and

$$N_R = \frac{VL\rho}{\mu} \quad \text{or} \quad \frac{VL}{\nu}$$

where (V) is a characteristic velocity and (L) is a characteristic length. Whether or not the dimensionless hydrodynamic equations can be solved, these numbers can often be used to relate results of hydraulic model tests to prototype conditions. The Froude number is the important parameter when gravity and free surface wave actions dominate. The Reynolds number is the important parameter when frictional and form losses dominate. Also the Reynolds number is used to indicate whether fluid flow is laminar or turbulent.

EFFECTS OF TEMPERATURE, PRESSURE, AND SALINITY ON DENSITY AND VISCOSITY

Both density and viscosity vary with temperature, pressure, and salinity. Thus the range of variations and the effect of these factors on fluid properties must be considered. For the area of the California Undersea Aqueduct, temperature of the water varies from about 44° F to 60° F. Pressure in terms of ocean depth will vary from 0 to about 600 feet. Salinity varies from about 33 to 35 p/t (parts per thousand by weight). Pressure will change the density (ρ) insignificantly because water is only slightly compressible. For example, seawater at 1 atmosphere, 56° F and 34 p/t, has a specific weight of 64.0 pounds per cubic foot. At the same temperature and at a depth of 300 feet, the specific weight increases by about 0.03 pounds per cubic foot. The effect of pressure on viscosity is even less significant. Therefore the fluid property curves in figures 1 and 2 show only the effects of temperature and salinity.

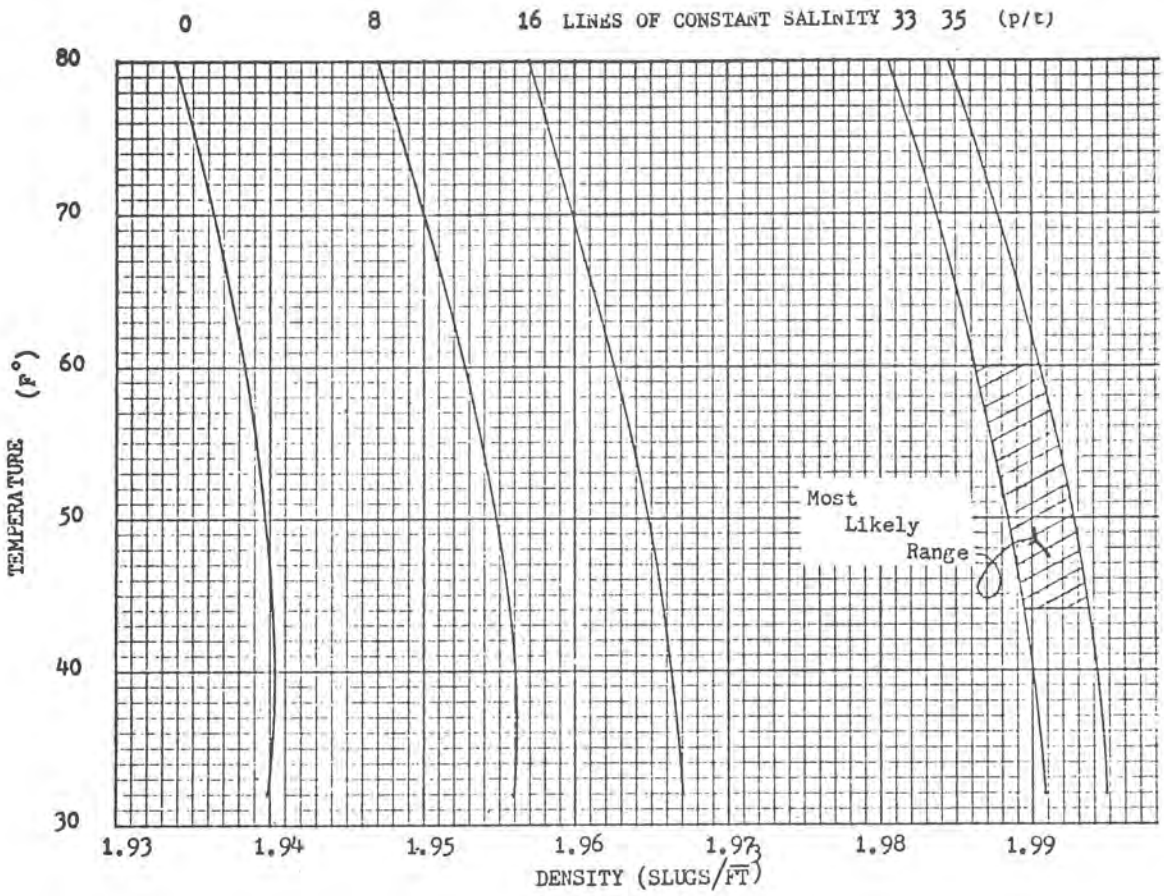

Figure 1 - Density versus temperature and salinity

Kinematic viscosity is plotted in Figure 2 for both freshwater and seawater. The most likely range from 33 to 35 p/t indicates that salinity has virtually no effect on viscosity and only temperature need be considered.

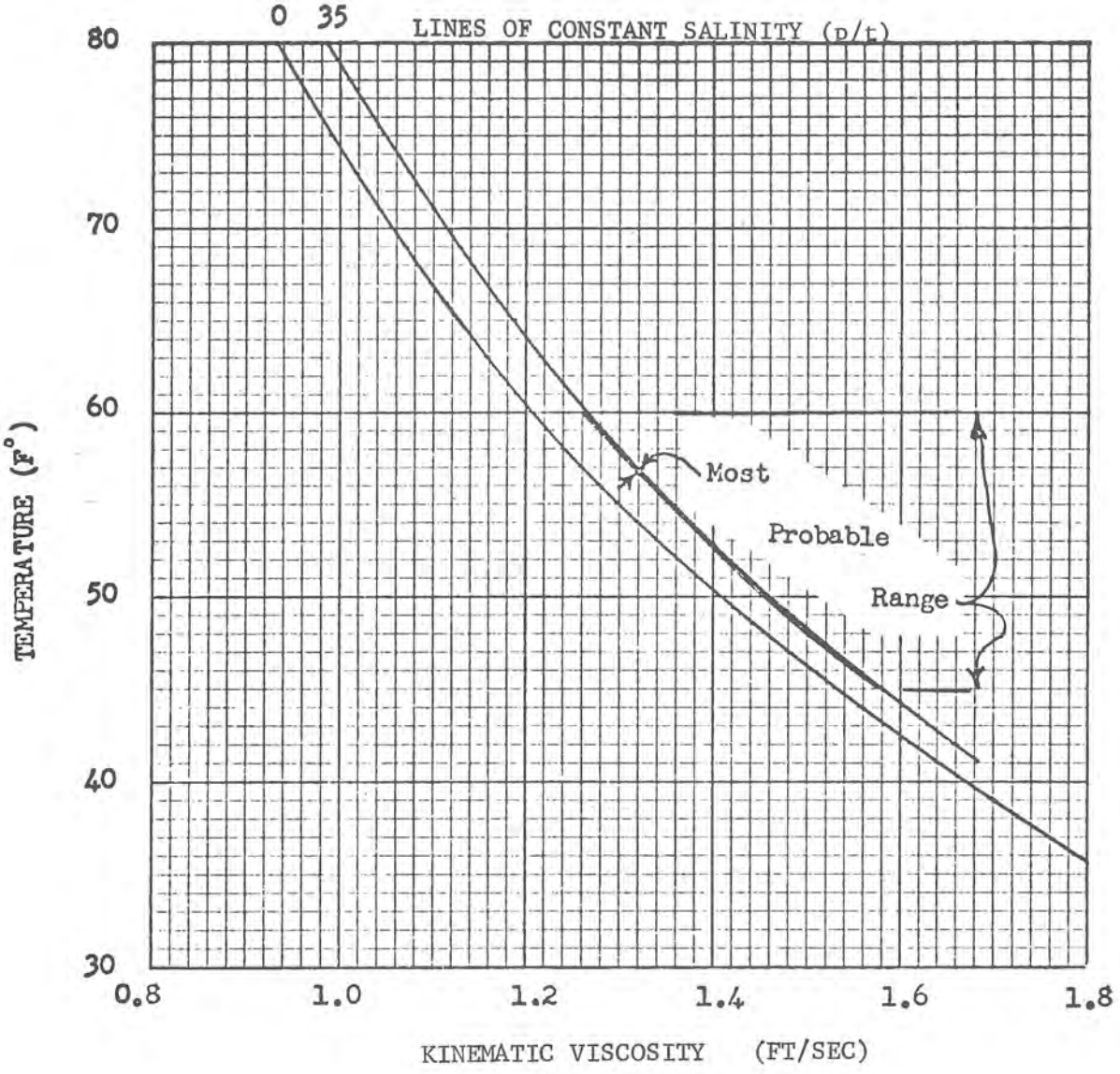

Figure 2 - Viscosity versus temperature and salinity

Fluid Properties

In figure 1 density is shown as a function of temperature and salinity. Curves are plotted for freshwater and seawater of 35 p/t. The curves for intermediate values of salinity are based on the assumption that density and specific weight of seawater at different salinities will vary similarly to aqueous solutions of (NaCl). The most probable range of density for water surrounding the Aqueduct is shown by the shaded area between 33 and 35 p/t and 44° F to 60° F. Specific weight can be calculated from density value by equation (3).

EFFECTS OF CONCENTRATED SUSPENDED SEDIMENT ON DENSITY

Fluids containing sufficient quantities of clay sediment can sustain small shears before yielding. These plastic suspensions have viscosity that applies only after yielding takes place, Bingham[4]. Dass, in Einstein et al[5], presents results of a deep marine sediment that passed through No. 140 sieve. From their data, values of relative density ratios as high as 1.10 and relative viscosity ratios as high as 2 may have application to sediment density flow and pipeline flotation problems.

J. D. Skoda, from Einstein et al[5], cites literature on turbidity current presumably containing larger size sediment than Dass; he infers densities up to 10 percent greater than the surrounding fluid and postulates densities up to 100 percent greater.

A high value of fluid density also has been cited for a pipeline that was lifted from a trench[6]. The water and suspended sediment were acting like a fluid having a density two times greater than that for freshwater.

BUOYANT FORCE

FORMULA FOR COMPUTING BUOYANT FORCE

When an object is immersed in a fluid, a buoyant force results. This force acts vertically upward through the object's center of gravity and is equal to the weight of fluid displaced by the object. The object will float or sink if it is lighter or heavier than the weight of the displaced fluid. For a pipe filled with freshwater and submerged in the ocean, the resultant buoyant force (F_{rb}) in pounds per linear foot of pipe is given as

$$F_{rb} = F_b - W_f - W_p = \frac{\pi}{4}D_o^2\gamma_s - \frac{\pi}{4}D_i^2\gamma_f - \frac{\pi}{4}(D_o^2 - D_o^2)\gamma_p \qquad (6)$$

where

D_o = outside pipe diameter, ft

D_i = inside pipe diameter, ft

γ_s = specific weight ocean water, lb/ft^3

γ_f = specific weight freshwater, lb/ft^3

γ_p = specific weight pipe material, lb/ft^3

F_b = buoyant force due to the weight of the displaced fluid, lb/ft

F_{rb} = resultant buoyant force of the conduit, lb/ft

W_f = weight freshwater in pipe, lb/ft

W_p = weight pipe, lb/ft

CONSIDERATION OF DENSITY OF TURBID WATER

Turbidity currents are distinguished from density currents in reference 7. A density current, sometimes called a suspension or turbidity flowage, is defined as a low-density (between 1.0 and

1.10 g/cm^3) current with velocity less than 6 knots. A turbidity current is defined as a high-density (1.10 g/cm^3 or denser) flow with velocity faster than 6 knots. Density currents have been observed near river sources with high sediment content. Turbidity currents have not been observed, but are believed to be located mainly along the continental slope and dissipate outward on the abyssal plain. Possibly slides or slumps occur more readily near or at mouths of submarine canyons which may terminate on the continental slope. Steepness of the continental slope is in the range of 45^o, thus encouraging sliding action. According to the literature, severe turbidity currents apparently will not occur at the pipeline location on the Continental Shelf.

Discussion of density and turbidity currents is found in the literature but the information is meager in regard to density values. The density of turbidity currents which have occurred in Lake Mead was 1 to 10 percent greater than the surrounding fluid. However, no substantial data were found for density of turbid ocean water[8].

BUOYANCY FOR THE BURIED CONCEPT

A buoyant force acts upon a buried underwater conduit. If a conduit is buried in sand, it is essentially immersed in a semifluid. Thus, hydrostatic pressure acts upon the conduit and equation (6) can be used to compute the resultant buoyant force due to water in the soil.

Buoyant Force

Liquefaction of the soil surrounding the conduit can cause a larger buoyant force on a buried pipe. A saturated mass of soil can suddenly lose its shearing strength when agitated by external forces and behave like a dense fluid[9]. Vibratory forces of earthquakes are known to cause liquefaction of submarine soils. Turbulence of water flowing in the conduit could vibrate the conduit and liquefy the soil. The pipeline industry refers to all undesirable motion of pipelines in saturated soils during and after laying as pipeline flotation[6].

An example of pipeline flotation[10] was a pipeline situated in a trench excavated along the ocean bottom. Backfilling was left to the natural sedimentation processes. Later, a storm of hurricane magnitude passed over the area. It was believed that under severe storm action, sand was transported into the trench. The resulting pressure surges and oscillating velocity of the waves kept the sand in a liquefied state. The medium surrounding the pipe had an approximate specific gravity of 2.0. About 3 miles of the pipeline floated from the bottom of the trench to the higher original ocean bed.

CONSIDERATION FOR THE PARTIALLY BURIED CONCEPT

If soil liquefaction occurs with a partially buried conduit, then the buoyant force (F_b) shown in figure 3 is composed of two parts where

Buoyant Force

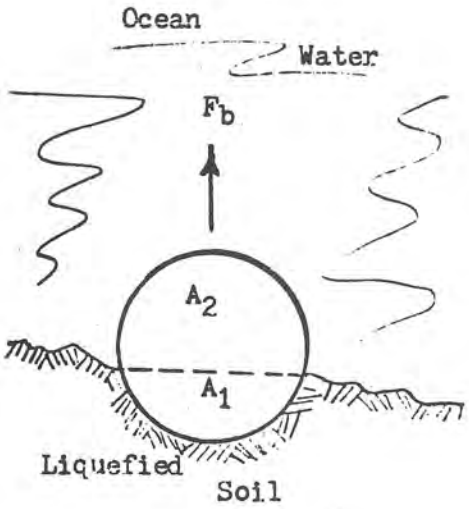

Figure 3 - Buoyant force in a two-liquid medium

$F_b = F_{b1} + F_{b2}$ and $A_1 + A_2 = \frac{\pi}{4} D_o^2$;

$F_{b1} = \gamma_1 A_1$ and $F_{b2} = \gamma_2 A_2$

F_b = buoyant force due to the weight of the two displaced fluids, lb/ft

F_{b1} = part of the buoyant force due to the conduit immersed in liquefied soil, lb/ft

F_{b2} = part of the buoyant force due to the conduit immersed in saltwater, lb/ft

A_1 = area of conduit immersed in the liquefied soil, ft^2

A_2 = area of conduit immersed in saltwater, ft^2

D_o = outside pipe diameter, ft

γ_1 = specific weight of liquefied soil, lb/ft^3

γ_2 = specific weight of ocean water, lb/ft^3

Depending on the combination of pipe weights and buoyant forces, the conduit will rise, sink, or be buoyantly neutral.

CONSIDERATION OF FOULING

Fouling is a hazard of unknown extent for the buoyant concept. Fouling is the accumulation of animals and plants when they grow on structures instead of on their natural anchorages in the ocean. "Accumulation of colonies of barnacles and mussels (specific gravities

1.2 and 1.4) and buoys can eventually sink a floating device unless sufficient extra positive buoyancy is allowed."[11]

Data about weights and thickness of marine fouling, or depths at which it occurs, are meager. Most fouling occurs in the upper 30 feet of water, but has been experienced 450 feet below the water surface. Weights are given[11] ranging from about 5 pounds of barnacles per square foot of surface in about a year to a maximum rate for mussel accumulation of 11 pounds per square foot per year with a maximum weight recorded as nearly 26 pounds per square foot in about 3 years. Fouling weights should be subtracted from the right side of equation (6), (page 13).

Growths and growth dimensions were given[11], for barnacles (up to 2 inches in diameter at base), sponge (up to 3 inches in height), jingle shells (up to 4 inches in diameter), sea anemones (some up to 5 inches in diameter at the base), and scallops (some up to 5 inches in diameter). One-foot thick mussel growths on navigation buoys have been occasionally reported. If the conduit is located at deeper depths (200 to 400 feet), the expected accumulations would be less.

Fouling affects the external roughness of the Aqueduct. At initial installation the outside pipe surface will be smooth, but the surface will soon become rough due to fouling. Therefore, the outside pipe surface must be considered as a "rough surface" when making drag force computations. It is expected that roughness projections could be in the order of 0.5 foot on a 30-foot diameter pipe.

PRESSURE VARIATION AROUND BODIES OF REVOLUTION

At low velocities the variation in pressure for potential flow around an immersed body is nearly hydrostatic. At high velocities unbalanced normal stresses are large and require detailed knowledge of pressure distribution and its temporal variation for determining structural stability, figure 4.

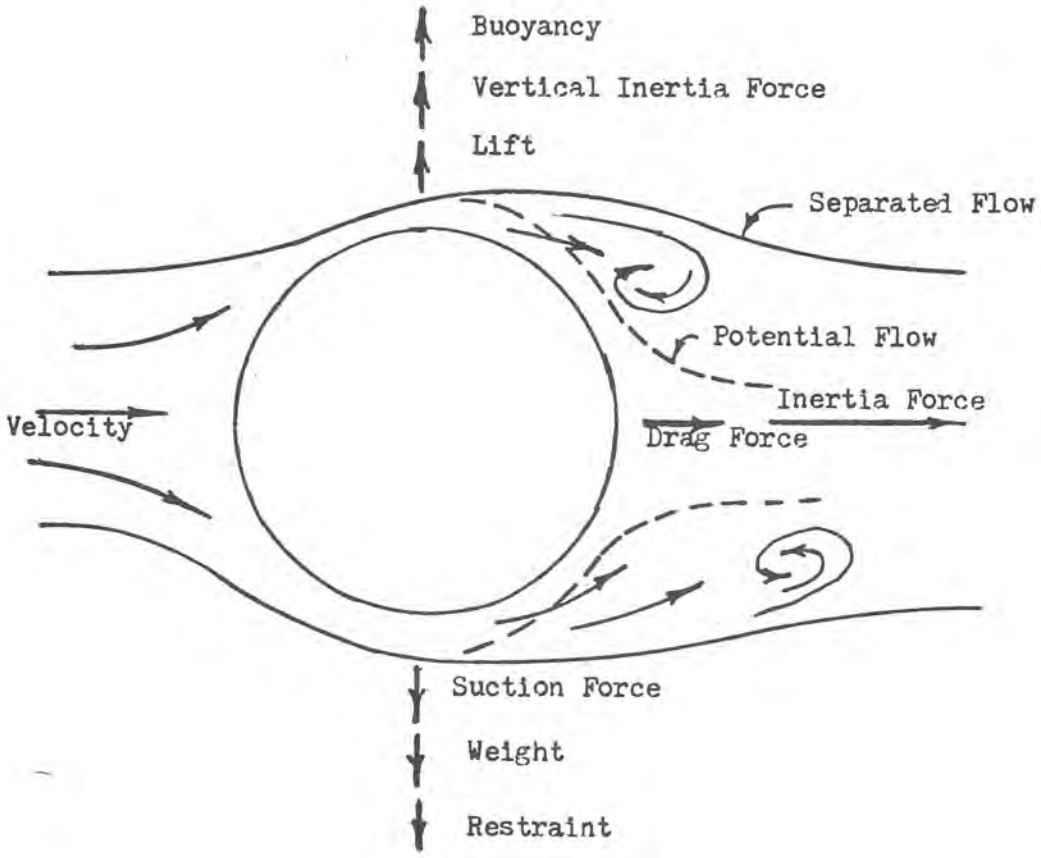

Figure 4 - Forces on buoyant cylinder

Hydrodynamic Forces on Conduit

The total resultant force on a body in flowing fluid is a summation of the components of all normal and tangential stresses on the boundary surface. These forces will be fluctuating for the velocities expected at the Aqueduct site.

MODELING HYDRODYNAMIC FORCES

Dimensional analysis leads to the conclusion that for geometrically similar systems, lift and drag forces may be related to Reynolds number. However, geometrical similarity must necessarily not only consider the body in question, but also its surface roughness and the proximity of other boundaries of the flow system. Reynolds number (R) is defined as

$$R_e,\ R_n = \frac{\rho VD}{\mu} \text{ where}$$

V = average approach velocity

D = diameter of cylinder

μ = dynamic viscosity of fluid

ρ = density

Reynolds number is actually the ratio of inertia force to the friction force.

The component of the resultant force in pounds in the direction of the undisturbed initial velocity is the drag (F_D), and the component perpendicular to the velocity is the lift (F_L). The dimensionless coefficients of drag and lift are defined for a unit length of cylinder as

$$C_D = \frac{F_D}{\rho\ DV^2/2} \qquad \text{and} \qquad C_L = \frac{F_L}{\rho\ DV^2/2}$$

Design of an undersea aqueduct requires a dynamic similarity between models used in obtaining experimental drag and lift coefficients and aqueduct pipes. According to the model law for predominant viscous force, Reynolds number for the model must be equal to Reynolds number for the prototype. Model cylinders have ranged from fractions of an inch to 24 inches in diameter. One set of data has information on coefficients measured from cylinders having diameters ranging from 3 to 24 inches[12]. Assuming a range of model cylinder sizes of about 0.25 to 2 feet for experimental data and 30 feet for the actual aqueduct, the range of model to prototype scaling is from 15 to 80. Because most of the data are on smaller size cylinders, an example will be based on the 0.25-foot diameter cylinder.

The drag and lift forces are dependent on the separation pattern of the flow around the cylinder. These patterns in turn are controlled by roughness, flow velocity, and turbulence level in the flow surrounding the cylinder. Low Reynolds numbers are usually associated with potential flows and high Reynolds number with separated flows. The force relationships are not well defined--especially in oscillating flows--because of the change in pressure distribution with the pattern of separation.

The dimensionless parameter, commonly used for relating the vortex frequency to Reynolds number is the Strouhal number

$$S = \frac{fD}{V}$$

where

f = measured vortex frequency

D = diameter of cylinder

V = average approach velocity

This relationship is not well defined in the transition range where pressure distribution changes as the flow clings or separates from the cylinder. Experimental values for the Strouhal number do not extend to the high Reynolds number required to model the Aqueduct.

The large difference between the diameter of the model cylinders, for which data are available, and the diameter of the Aqueduct is a basis for much doubt on the validity of extrapolating the drag, lift, and mass or inertia coefficients from a model to a prototype force. However, because data from large cylinders were not available, the small model data discussed in this section are used in recommending values of the coefficients, table 1.

BUOYANT CONCEPT

Drag Force

The major force on a pipe in a steady current is the drag force. The drag force has two additive components, a form or pressure drag, and a skin friction distribution around the cylinder.

Table 1. Summary of recommended drag C_D, lift C_L, and inertia C_M coefficients and Strouhal numbers

Coefficients	Recommended	Probable range
BUOYANT CONCEPT:		
Drag		
Single cylinder		
Normal flow	1.2	0.25 to 1.3
45°	(3 max.)	
Paired cylinders		
Separation 4D		
Upstream	1	
Downstream	0.5	
Lift		
Single cylinder	0.5	h/d = 0, 0.6 h/d = 0.3, 0.1
Paired cylinders		
Separation		
4D h/d = 0.02		
Upstream	0.7	
Downstream	0.4	
Inertia		
Single cylinder	2	0.7 to 5
Strouhal number	Compare to pipe natural bending frequency	0.2 to 0.45

Table 1 (Continued)

Coefficients	Recommended	Probable Range
CONTACT OR PARTLY EMBEDDED CONCEPT:		
Drag		
Single cylinder	0.9	0.85 to 0.93
Lift		
Single	1.5	1.48 to 1.11
Inertia	NOT KNOWN	
Strouhal number		
Single Paired	Compare to pipe natural bending frequency	Variation in ratio of natural frequency to vortex frequency f/fs = 2 to 5
Variation with current angle	90^{o} 0.2 60^{o} 0.1	

Roughness of a 150-mm cylinder surface was studied by Achenback[13]. His studies indicated a maximum frictional drag of the order of 2 to 3 percent of the total drag. Pressure distribution or form drag appeared to be the predominant part of the total drag.

Marine growths on the pipe roughen the surface, although the character of the roughness and the effect on the total drag have not had thorough study. The estimated possible thickness of the growths is up to 6 inches, or a relative roughness of 1700×10^{-5}. Data[13] indicates that for a roughness of 2000×10^{-5}, total drag would not be materially affected except by the increase in total projected area and turbulence level of the flow around the surface of the pipe.

For steady flow passing a fixed pipeline, coefficient of drag most probably would vary from 0.25 to 1.3. The 0.25 value occurs in the critical range or the shift of the flow pattern from partially to fully separated flows. The higher values in table 1 are recommended for appraisal design use.

Changes in drag coefficient on a smooth upstream or downstream cylinder of a pair show a wide variation for the small Reynolds number range of the study[14]. The spacing between cylinders and distance from a boundary both affected the drag force.

Lift Force

A suspended cylinder outside the influence of other boundaries or objects experiences no lift force in potential flow. In separated

flow, a periodic upward and downward force is imposed by the periodic shedding of vortexes, that is, changes in the lift force.

In an asymmetrical flow produced by a flat boundary near the cylinder, a downward force or negative lift is imposed on the pipe. Velocities are increased between the pipe and boundary, producing an unbalance of pressure toward the flat boundary. Analytical and experimental evaluations have been made of the change of the lift coefficient for single and paired cylinders adjacent to boundaries. Experimental data for Reynolds numbers from 33,200 to 150,000 vary from 0.3 to 0.6 for a cylinder near the boundary and from 0.1 to 0.35 at 0.3 of a diameter from the boundary[14, 15].

The increase in lift on an upstream cylinder in a pair, caused by the presence of a cylinder downstream, are given in reference 14 for small models and low Reynolds numbers. The lift coefficients include the proximity effects of a boundary as well as of another cylinder.

Oscillating Forces

A primary characteristic of the flow past a stationary cylinder is the lateral pendulation of the separation zone as a vortex is shed from alternating sides of the flow centerline. Experiments have generalized the characteristics of the shedding frequency in terms of the cylinder Reynolds number and the Strouhal number (S) as previously cited.

Hydrodynamic Forces on Conduit

Although an abundant amount of information is available on vortex frequency, application of the results may be limited by the large Reynolds number for aqueduct pipeline. Strouhal numbers range from about 0.2 to 0.45, and for Reynolds numbers from 10,000 to 1,500,000. Measurements at higher Reynolds numbers indicate a decrease in Strouhal number to about 0.25. Selection of a Strouhal number from these small model data to apply to the large aqueduct is risky. Calculating the Strouhal number using the natural bending frequency of the pipeline would indicate a critical Strouhal number. Coincidence of the number with one in the range indicated by experimental investigations would be cause for an extensive study of the possible oscillation of the Aqueduct.

Forced oscillation of a flexible cylinder, e.g., a tethered aqueduct pipeline, by waves could cause serious bending movements if the natural period of elastic oscillation is in resonance with the vortex trail and wave velocity periods. The force exerted by the water on the moving pipeline contains two parts, one of which depends on the form drag, and the other on the displaced water.

The direct fundamental approach represents the differential total force on the cylinder as the sum of the differential drag and inertia force components:

$$dF_T = dF_D + dF_I \quad \text{(Morison Formula)}$$

The components dF_T and dF_I are defined

$$dF_D = C_D \rho D \frac{u|u|}{2} ds$$

$$dF_I = C_M \rho \frac{\pi D^2}{4} \dot{u} ds$$

where

D = diameter of pipe

ds = differential of surface

ρ = density of water

u = instantaneous horizontal velocity of water particle

$\dot{u}$ = instantaneous horizontal acceleration of water particle

C_D = hydrodynamic force coefficient, the drag coefficient

C_M = hydrodynamic force coefficient, the inertia or mass coefficient

The equation for the drag force component is the usual representation of the force resulting from the steady flow, which was discussed in the previous section on drag. The absolute value symbols in the (F_D) equation insure that the drag force component is in the same direction as the velocity.

Measurements of drag forces on cylinders subject to wave velocities show a large scatter apparently caused by turbulence near the cylinder. A steady state vortex-shedding period cannot occur because of the oscillating nature of the wave velocity. Thus in the presence of a current and oscillating wave velocity, wide variations occur in the drag force. Data for waves greater than 10 feet, cylinders ranging

from 7 to 13 inches in diameter and between Reynolds numbers from 300,000 to 700,000 had a coefficient drag scatter from 0.1 to 2.0[16].

Flow patterns resulting from the movement of a cylinder in the surrounding water, in unsteady and oscillating flows, are related through the "inertia" or "mass" coefficient. Because of the oscillating motion of both the pipe and water, the effects of such motion are not well known.

An early theoretical and experimental study resulted in agreement of the computed and measured forces on a cylinder in a wave tank[17]. The Morison type equation was used to find the total force on the cylinder. No steady or unsteady currents were imposed on the simple sinusoidal currents in a rectangular basin.

Studies in later years were extended by investigating the forces on single and paired cylinders in laboratory and ocean environments[18, 19, 20, 21]. These studies further reinforced the doubt of assuming a (C_D) value for steady flow applied to a cylinder in reversible accelerating flow. This uncertainty as well as the wide variance of values for both (C_D) and (C_M) indicate caution should be exercised in using the information in a model to aqueduct conformance.

A summary[22] of (C_D) and (C_M) coefficients for cylinders indicates an average of ($\overline{C}_D = 1.05$) and ($\overline{C}_M = 1.40$) would be a first approximation, in an appraisal design of the buoyant aqueduct. A mean value of ($\overline{C}_M = 2.5$), standard deviation of 1.2 was calculated from data by Bearman[23]. This mean, in a range of (C_M) values from

0.7 to 5.5, indicates a much larger inertia effect. Thus, a maximum (C_M) value appears to be greater than 5 or about 2.5 times the theoretical value of 2. Information reviewed generally indicates that an inertia coefficient value ($C_M = 2$) should be used in the appraisal study of the Aqueduct.

Before design forces on a large aqueduct can be calculated with confidence, additional investigation of larger models, onsite testing, or further analysis of reported results may be necessary. Further investigations may resolve the inconsistencies by rigorous control of experimental facilities.

This area of the hydrodynamic design of structures in the ocean has been reviewed by several organizations, and their publications[15, 24, 25, 26] offer valuable reference information. This portion of the design study of the buoyant concept of the Aqueduct should be given comprehensive study, because of the modes of movement possible from a semirigid structure. Forces varying in magnitude and direction at sections of the pipe throughout its length could produce a highly complex dynamic behavior of the Aqueduct.

CYLINDER IN CONTACT OR PARTLY EMBEDDED IN BOUNDARY

Drag, Lift, and Oscillatory Forces

Design of the Aqueduct could require the pipe to be restrained in contact or partly buried in the ocean floor.

Asymmetry of flow will produce forces of lift, drag, and oscillation to be balanced by the restrained structure. Studies of forces

for the pipe configurations of boundary in contact and partly buried appear to have been minimal[19, 26].

A discussion[19, 22] suggests that the values of (C_D), (C_L), and (C_M) recommended from the studies are too low. Values of ($C_D = 0.05$), ($C_L = 0.5$), and ($C_M = 1.5$) appear to have been used in the analysis, but larger values of ($C_D \geq 1$), ($C_L \geq 1$), and ($C_M \geq 2.5$) were suggested.

Six- and 10-inch cylinders in a Venturi-shaped flume were used for an investigation of lift and drag coefficients[26]. Pressures were measured at the cylinder surface, and velocities in the surrounding flow.

Values of (C_D) in the range 0.9 to 0.55, and (C_L) in the range 1.3 to 0.8 for Reynolds numbers ranging from 60,000 to 300,000 resulted from the investigations. No inertia or mass coefficient information was included in the results. Additional experiments[27] resulted in drag and lift coefficients of ($C_D = 0.85$ to 0.93) and ($C_L = 1.48$ to 1.11) for a Reynolds number range from 53,000 to 97,000. The lift and drag force exerted on the cylinder will be oscillatory. Vortex formation in the wake of the cylinder will be periodic. The period of the force may be inferred from the investigations of vibrating cylinders having different natural vibrating frequencies and cylinder material to fluid mass ratios (M)[27]. Extrapolations of the data were made for a single cylinder in contact with the boundary, but none have been made for paired cylinders. Reynolds numbers for measuring the frequency ratios were small, the

largest being about 25,000. Mass ratios were scaled to represent steel pipes carrying oil, ($1<M<3$). The model ratio ranged from ($0.78 \leq M \leq 2.4$) and the natural frequency from about 4.5 to 24.5 cycles per second. The stiffness of the model was increased, thus increasing the natural frequency, over a Reynolds number range of 3,000 to 25,000. Model-to-aqueduct scaling (1.5-inch cylinders to the 30-foot-diameter) for an aqueduct in contact or partly embedded in a boundary is risky because the Reynolds number for the Aqueduct is about 10 million.

One conclusion indicated that the natural bending frequency of the cylinder of a segment between anchor blocks should exceed 5 cycles per second to avoid significant midspan deflections. Paired cylinders showed a frequency ratio greater than 5 as the cylinders were placed 0.25 of the diameter from the boundary.

For a cylinder on or embedded in a boundary, available information on drag, lift, and inertia coefficients is meager. To improve the reliability of these coefficients, extensive investigations are needed on larger cylinders near boundaries. These studies should include thorough investigation of the interaction of the pipe moving in an oscillating flow of water.

EFFECT OF CURRENTS ON AN ANGLE TO CYLINDER

Currents will flow past the cylinder at an angle in the buoyant, in contact, and partly embedded concepts of aqueduct construction.

A small amount of information was available for a cylinder remote from a boundary[28, 29].

Chiu and Lienhard[28] concluded that the separation along a cylinder was independent of the flow angle, and would occur beyond the separation point of the flow component across the cylinder. Thus, water particles in the wake followed counterrotating corkscrew paths within the upper and lower rows of the vortex paths. For the crosswise component, the Strouhal number and pressure drag coefficient were evaluated as though the spanwise flow did not exist. Strouhal numbers measured for Reynolds numbers between 3,900 and 21,999 gradually diminished from 0.2 to 0.0 as the current angle approaches the direction of the pipe, with the Strouhal number of about 0.1 at a 60^{o} current angle.

Wilson and Caldwell[14] show that drag coefficients for yawed cylinders at angles between 45^{o} and 90^{o} range from about 1 to 3 for Reynolds numbers between 33,000 and 57,000. The direction of the drag force is the same as the undisturbed velocity. Slight decreases in the coefficient were indicated as the space was decreased between the cylinder and the boundary. In this study average values of drag coefficient were calculated. Information was not available for evaluating a drag and mass or inertia coefficient in the Morison equation for cylinders inclined to the current direction.

WATER MOVEMENT CAUSED BY WAVES AND EFFECT ON THE CONDUIT

AIRY WAVE THEORY

Ocean waves usually are very irregular. A wave train can have superpositions of different waves with various wave heights and lengths. A mathematical theory has not been developed that precisely describes all the diverse features of natural wave action in water. Many theories of varying complexity and difficulty have been developed, however, to describe water movement caused by waves.

For engineering purposes, the Airy equations are often used. A description of the theoretical derivation of the Airy equation is given in Ippen[30]. These equations are recommended for use in appraisal stage design because (1) these equations are the most convenient to use, and (2) for defining velocities occurring within the lower half of the water depth, the results appear as dependable as those from other theories.

The decision to use Airy wave theory was made after considering references 31 and 32. The maximum horizontal and vertical water velocities occurring beneath waves have been measured in a wave tank for a (d/L) value of approximately 1/10[31]. The theory agrees favorably with the measured horizontal velocities in the lower 1/2 depth range; for vertical velocity results are about 30 percent smaller. Thus, the simple Airy theory may be applied at the bottom especially for horizontal forces. Horizontal particle velocities for various wave theories are compared in reference 32. For the lower 1/3 depth range, the Airy theory agrees closely with two other wave theories,

while a third wave theory shows higher velocities. Reference 32 concludes that whenever inertia or acceleration forces dominate, a first-order wave theory such as the Airy's is probably sufficient. Wave calculations for a large diameter pipe show that acceleration forces are predominant.

A sine wave profile shape is used for deriving the Airy equations, (figure 5). The wave length (L) is the horizontal distance between wave crests, and the wave height (H) the vertical distance from trough to crest. The wave period (T) is the time required for a wave crest to travel the distance of one wave length.

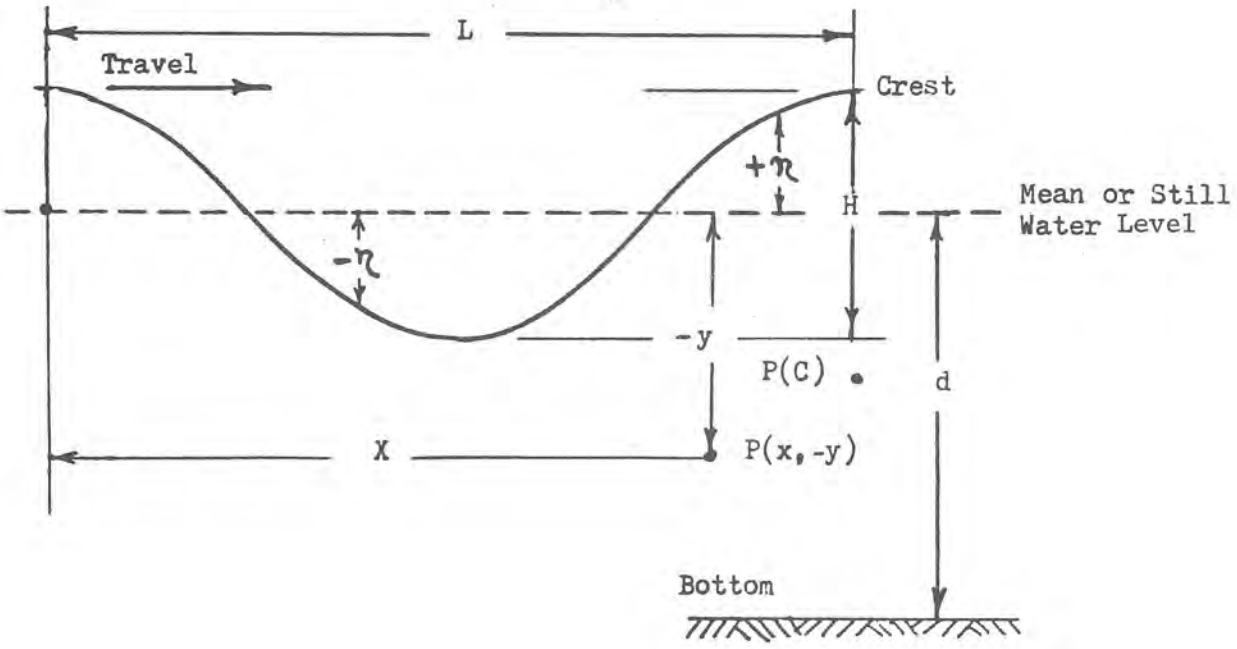

Figure 5 - Definition sketch for waves

The equation

$$n = a(\cos \theta)$$

describes the wave profile on the water surface where (n) is vertical distance water surface is from mean or still water level.

Wave action formulated by the Airy equations is periodic in nature. A cycle of wave action occurs over and over again. Phase angle is defined:

$$\theta = 2\pi \left(\frac{x}{L} - \frac{t}{T}\right)$$

Where (x) is horizontal distance measured in the direction of wave propagation and (t) is time measured from some wave crest selected to be at (x = 0). The phase angle varies between (0 to 2π) or multiples of (2π) for one cycle of wave action. The cosine of the phase angle performs a cycling function to parameters of wave action. The phase angle equation can be simplified when the wave acts perpendicular to the pipe. The centerline can be called (x = 0). Then the phase angle equation is written as

$$\theta = 2\pi \left(- \frac{t}{T}\right)$$

Wave celerity is the velocity at which the wave travels across the water surface. By definition the wave celerity is

$$C = \frac{L}{T}$$

By Airy theory, celerity also follows the relationship of

$$C^2 = \frac{Lg}{2\pi}\tanh\left(\frac{2\pi d}{L}\right)$$

where (g) is the acceleration of gravity, (d) is the depth from mean water level to the bottom.

WAVE WATER PARTICLE ORBITS

Waves are usually classified according to the ratio of depth to wave length.

Deep	Intermediate	Shallow
$d/L \geq 1/2$	$1/2 > d/L > 1/20$	$d/L \leq 1/20$

As waves travel along the water surface, the water particles beneath the waves experience an orbital motion. A water particle travels once around its orbit path during the wave period (T). The magnitude and shape of the orbital path vary with distance below the water surface and (d/L) ratio. Orbit paths change shape as a wave progresses toward the shore (figure 6). For a deep water wave, say for a (d/L) ratio of 1, the orbits are circular and their size becomes expotentially smaller with increasing depth below the water surface. For a (d/L) ratio of 1/2, the orbital motion extends to the bottom. Downward movement of the orbital water motion is then inhibited, and the motion is mainly linear oscillation in the horizontal direction. The orbits are elliptical near the bottom and may be circular near the water surface. As waves move into shallower water, the major axes of the elliptical elongations become increasingly

larger. In shallow water there is less change with decreasing depth in the horizontal portion of the displacement magnitude.

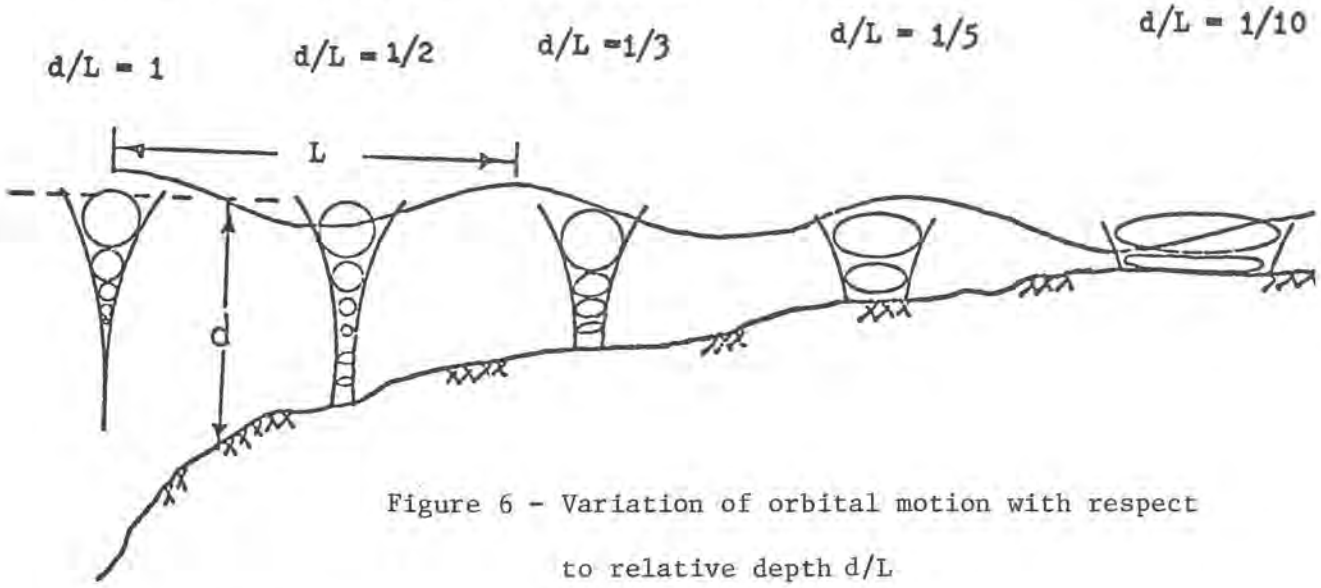

Figure 6 - Variation of orbital motion with respect to relative depth d/L

WAVE EQUATIONS

The basic Airy wave equations are listed next, followed by pertinent nomenclature and definitions. Wave forces must be determined from velocities, and accelerations determined from these equations. The design concept, and whether the Aqueduct can move or respond to wave forces, must be considered when these equations are used for appraisal design.

Water Movement Caused by Waves and Effect on the Conduit

$$\theta = 2\pi\left(\frac{x}{L} - \frac{t}{T}\right)$$

$$\eta = a(\cos\ \theta)$$

$$C = \frac{L}{T}$$

$$C^2 = \frac{g}{k}\ \tanh\ (kd)$$

$$\varepsilon_x = -a\left[\frac{\cosh\ k(d+y)}{\sinh\ kd}\right]\sin\ \theta$$

$$\varepsilon_y = a\left[\frac{\sinh\ k(d+y)}{\sinh\ kd}\right]\cos\ \theta$$

$$V_x = a\left(\frac{2\pi}{T}\right)\left[\frac{\cosh\ k(d+y)}{\sinh\ kd}\right]\cos\ \theta$$

$$V_y = a\left(\frac{2\pi}{T}\right)\left[\frac{\sinh\ k(d+y)}{\sinh\ kd}\right]\sin\ \theta$$

$$A_x = a\left(\frac{2\pi}{T}\right)^2\left[\frac{\cosh\ k(d+y)}{\sinh\ kd}\right]\sin\ \theta$$

$$A_y = -a\left(\frac{2\pi}{T}\right)^2\left[\frac{\sinh\ k(d+y)}{\sinh\ kd}\right]\cos\ \theta$$

$$p = \gamma\left[a\frac{\cosh\ k(d+y)}{\cosh\ kd}\ \cos\ \theta - y\right]$$

NOMENCLATURE AND DEFINITIONS

x - horizontal coordinate, ft

y - vertical coordinate, ft

d - water depth, distance from mean water level to the bottom, ft

η - vertical distance or displacement of the water surface from mean water level, ft

H - wave height, ft

a - wave amplitude, $a = H/2$, ft

L - wave length, ft

T - wave period, sec

C - wave celerity, ft/sec

g - acceleration of gravity, ft/sec^2

t - time measured from the instant that a wave crest is located at $x = 0$, sec

θ - phase, angle $\theta = 2\pi(x/L - t/T)$, radians

ε - water particle orbit displacement, ft

V - water particle orbit velocities, ft/sec

A - water particle orbit accelerations, ft/sec^2

k - radian "wave number," $k = 2\pi/L$

p - pressure, lb/ft^2

γ - specific weight, lb/ft^3

Use of the Morison Formula

When there is pipe movement, relative velocity and acceleration should be used in the Morison Formula

$$\vec{F}_T = K_D(\vec{V}_R^2) + K_A\vec{A}_R$$

$$K_D = \frac{\rho C_D D}{2} \quad , \quad K_A = \frac{\pi \rho C_m D^2}{4}$$

The relative velocity and acceleration are

$$\vec{V}_R = \vec{V}_p - \vec{V}_c \qquad \text{and} \qquad \vec{A}_R = \vec{A}_p - \vec{A}_c$$

where

$\vec{V}_R$ - relative velocity vector

$\vec{V}_p = \vec{V}_x + \vec{V}_y$ - particle velocity vector

$\vec{V}_c$ - conduit velocity vector due to pipe movement

$\vec{A}_R$ - relative acceleration vector

$\vec{A}_p = \vec{A}_x + \vec{A}_y$ - particle acceleration vector

$\vec{A}_c$ - conduit acceleration vector due to pipe movement

C_D - coefficient of drag

C_m - coefficient of mass

One difficulty is determining what $(\vec{V}_c)$ and $(\vec{A}_c)$ values to use in the Morison Formula when computing the force acting upon the pipe.

Water Movement Caused by Waves and Effect on the Conduit

Forces of wave action flex and move the pipe; this movement is in turn structurally transferred to the tethered supports; these respond by providing a restoring force which moves the pipe. Thus to determine pipe movement, the force acting on the pipe must be known, yet this force is interrelated with and is a function of pipe movement.

SCOUR

BACKGROUND

Scour is a complicated interplay between sediments, structures, structural responses, and flow dynamics[33]. The interaction is complicated by the loose boundary between the flowing fluid and the sediment. Flow can change the shape of sediment beds by scour or aggradation. The change in bed shape changes the flow.

Sediment has an infinite combination of grain sizes that need to be expressed by statistical distributions of grain size (d) which partially classifies them. Sediments are further complicated by variation of cohesiveness expressed by the Plastic Index (PI) and the Liquid Limit (LL) which also partially classifies the soils. Resistance to scour must be expressed in terms of these soil properties and the state of consolidation.

Fluid shear at the sediment boundary, lift, and turbulence initiate the transport of sediment. To determine average shear in ocean flows, velocity distributions need to be known. Turbulence is described as statistical distributions of eddy sizes and velocity fluctuations. Turbulence causes random fluctuation of shear, lift, and drag forces acting on the sediment particles. Particles can slide, roll, bounce, move as bed form waves, or travel in suspension. The statistical nature of turbulence, sediment, and its movement is the reason why Einstein[33] used probabilistic models in developing his sediment transport theory and functions.

Scour

Structures have various sizes and shapes that accelerate the main flow and change the turbulence characteristics of the flow near the structure whether responding or not. Scour near structures is almost exclusively studied by models requiring compromising model distortions and applies only to cohesionless sediment. No distortion model laws are known for modeling scour with cohesive soils. Knowledge of sediment transport, bed forms, scour, and deposition is rather limited and comes mostly from experience with channelized flow with freshwater rather than seawater.

For the ocean environment, there is very little documented experience, and capability of predicting scour on the ocean bottom is further limited by complicated reversing and oscillating flows caused by tides and surface waves that are superimposed on the main ocean currents.

APPLICATION

Data on marine soils and bottom ocean currents suitable for use in making scour predictions are scarce. During the appraisal design stage, scour cover will probably have to be eliminated by providing adequate Aqueduct foundation and anchorage, deep enough in the ocean bed or attached to bedrock. Oil companies commonly require 10 feet of cover to provide protection from the disturbance caused by the presence of their structures. Hopefully at this point in the appraisal, further worry or concern with scour may have been eliminated. If the critical scour criteria indicates scour and the

soil is noncohesive, then checking the possible use of dimensionless scour data is recommended. Only for advanced design stages beyond the appraisal stage should the more elaborate computational methods be considered.

RELATIVE SCOUR RESISTANCE IN TERMS OF SOIL CLASSIFICATION

Ranking by Unified Soil Classification Groups

Through experience, engineers have developed concepts of relative resistance of soils by categories to erosion. For example, Bureau of Reclamation soils engineers have ranked[34] the relative resistance of different soil types in table 2. This ranking is for canals where the embankments have been compacted or consolidated. The degree of compaction in ocean sediment is one of the more important unknowns when appraising scour. However, the ranking in the table is probably adequate for cohesionless soils and for thoroughly consolidated cohesive soils.

Ranking in Terms of Soil Plastic Properties

For soils with over 50 percent of their grain diameters less than 0.074 mm, plastic properties can contribute in varying degrees from just slightly adding to erosion resistance to being the dominant source. Plastic soil properties are expressed by the Atterberg limits as follows:

1. The Liquid Limit (LL), the water content percent dry weight that marks the separation between acting like a liquid or a plastic.

Table 2. Soil classification[34]

MAJOR DIVISIONS OF SOILS			TYPICAL NAMES OF SOIL GROUPS	GROUP SYMBOLS	EROSION RESISTANCE
COARSE GRAINED SOILS — More than half of material is larger than No. 200 sieve size (The No. 200 sieve size is about the smallest particle visible to the naked eye)	GRAVELS — More than half of coarse fraction is larger than No. 4 sieve size (For visual classifications, the ¼" size may be used as equivalent to the No. 4 sieve size)	CLEAN GRAVELS (Little or no fines)	Well graded gravels, gravel-sand mixtures, little or no fines	GW	2
			Poorly graded gravels, gravel-sand mixtures, little or no fines	GP	3
		GRAVELS WITH FINES (Appreciable amount of fines)	Silty gravels, poorly graded gravel-sand-silt mixtures	GM	5
			Clayey gravels, poorly graded gravel-sand-clay mixtures	GC	4
			Gravel with sand-clay binder	GW-GC	1
	SANDS — More than half of coarse fraction is smaller than No. 4 sieve size (For visual classifications, the ¼" size may be used as equivalent to the No. 4 sieve size)	CLEAN SANDS (Little or no fines)	Well graded sands, gravelly sands, little or no fines	SW	8
			Poorly graded sands; gravelly sands, little or no fines	SP	9 coarse
		SANDS WITH FINES (Appreciable amount of fines)	Silty sands, poorly graded sand-silt mixtures	SM	10 coarse
			Clayey sands, poorly graded sand-clay mixtures	SC	7
			Sand with clay binder	SW-SC	6
FINE GRAINED SOILS — More than half of material is smaller than No. 200 sieve size (The No. 200 sieve size is about the smallest particle visible to the naked eye)	SILTS AND CLAYS Liquid limit less than 50		Inorganic silts and very fine sands, rock flour, silty or clayey fine sands with slight plasticity	ML	—
			Inorganic clays of low to medium plasticity, gravelly clays, sandy clays, silty clays, lean clays	CL	11
			Organic silts and organic silt-clays of low plasticity	OL	—
	SILTS AND CLAYS Liquid limit greater than 50		Inorganic silt, micaceous or diatomaceous fine sandy or silty soils, elastic silts	MH	—
			Inorganic clays of high plasticity, fat clays	CH	12
			Organic clays of medium to high plasticity	OH	—
HIGHLY ORGANIC SOILS			Peat and other highly organic soils	Pt	**

**Numbers above indicate the order of increasing values for the physical property named indicate relative suitability (1 = best)

2. The Plastic Limit (PL), the boundary between acting like a plastic or a solid.

3. The Plastic Index (PI), which is the difference between (LL) and (PL), and is the range of water content through which the soil has plastic characteristics.

Reference 34 gives the relative resistance of cohesive soils in terms of the Liquid Limit (LL) and the Plastic Index (PI).

TYPES OF SOIL ON THE CONTINENTAL SHELF

To apply data in table 2, soil samples must be obtained at the site or existing sampling records must be used. There is not much information about Continental Shelf sediments. Appendix IV discusses soil types within the 3-mile limit and estimates distribution of soil types along the 60-foot and 300-foot contour lines on the Continental Shelf.

CRITICAL SCOUR CRITERIA

Background

In order to quantify scour and transport criteria, soil types or soil properties must be related to flow dynamic properties. For cohesionless soils, it is generally accepted that the weight (W) of the largest sediment grain transported is proportionally related to velocity (V) as follows:

$$W \alpha V^6 \qquad (7)$$

The quantity of sediment transported (q_s) is proportionally related[29, 35] as follows:

$$q_s \alpha V^n$$

where the exponent (n) is approximately equal to 1/4. Equation (7) suggests the possibility of a critical velocity (V_{cr}) that will just move a particle of diameter (d). Assuming all the particles are spheres with constant specific weight, then

$$W \alpha d^3$$

which combined with equation (7) results in

$$V_{cr} \alpha d^{1/2}$$

Shear and shear fluctuations at the sediment boundary are considered the dominant factors in initiating sediment movement. For flow in canals and rivers, assuming normal flow, average shear can easily be determined from a free body diagram. Then

$$\tau = \gamma_f D\ S \qquad (8)$$

τ - the boundary shear lbs/ft^2

D - depth (ft)

S - slope of energy gradient

γ - specific weight, lbs/ft^3

f - subscript denoting fluid

Excepting turbidity and density currents, flow is not necessarily in the direction of the bottom slopes. Therefore, no energy slope (S) can be easily assigned to a particular portion of the ocean bed. Shear must be obtained from a velocity distribution law, with at least two measured velocities at different elevations near the bed required. Boundary shear can then be expressed as

$$\tau = \rho \left[\frac{V_2 - V_1}{5.75 \log_{10} \frac{Z_2}{Z_1}} \right]^2 \qquad (9)$$

where (Z_1) and (Z_2) are elevations above the bed corresponding to (V_1) and (V_2). Equations 8 and 9 indicate that tractive force is proportional to the square of velocity. Thus, there is the possibility of a critical tractive force (τ_{cr}) or shear that will just move a particle of diameter (d).

When over 50 percent of soil particles are less than 0.074 mm, cohesion should be considered. Sometimes the effects of cohesion are incorporated into an analysis by assuming that it is defined by grain size only. More complicated approaches can be used that include up to as many as nine soil variables.

Turbulence contributes in initiating movement and is very important in keeping particles in suspension once they are suspended. Turbulent intensity (ε_t) is expressed as

$$\varepsilon_t = \frac{\sqrt{\overline{V'^2}}}{V_m}$$

where (V') is velocity fluctuation about (V_m) the mean velocity. Values of (ε_t) have been measured from 0.03 up to 0.07, with 0.1 the value at which velocity fluctuations can no longer be considered part of the main flow[36]. Graf[37] indicates that the maximum instantaneous velocity fluctuation (V_{mb}) near the bed can be 1.75 times the average

velocity. Since (τ) is proportional to velocity squared, then maximum instantaneous shear fluctuation can be about three times the average shear. The critical tractive force for noncohesive soils versus mean grain diameter is plotted in figure 7.

Critical Tractive Force Versus Grain Size for Noncohesive Soils

Lane[38] summarizes a considerable number of the investigations concerning critical scour criteria; tables 3 through 7 were taken from his work.

Table 3 is a comparison of Etcheverry's maximum allowable velocities and tractive forces for various materials. Table 4 compares Fortier and Scobey's limiting velocities with tractive force values for straight channels after aging. USSR data on permissible velocities for noncohesive soils is presented in table 5; table 6 gives the correction factor for depth. Table 7 shows the USSR limiting velocities and tractive forces in cohesive soil.

Sediment Entrainment Function

The concept of a dimensionless entrainment function was first used by Shields[39] and is generally accepted for uniform soils or single grain sizes. Besides giving a yes-no determination of bed transport, Shields' curve can be used to indicate bed form and transport mode that will occur. Gessler[40] shows that the average bottom shear is equal to critical shear for a given grain size when the probability (q) of remaining still is 0.5. He then determines that this definition is independent of grain distributions or armoring.

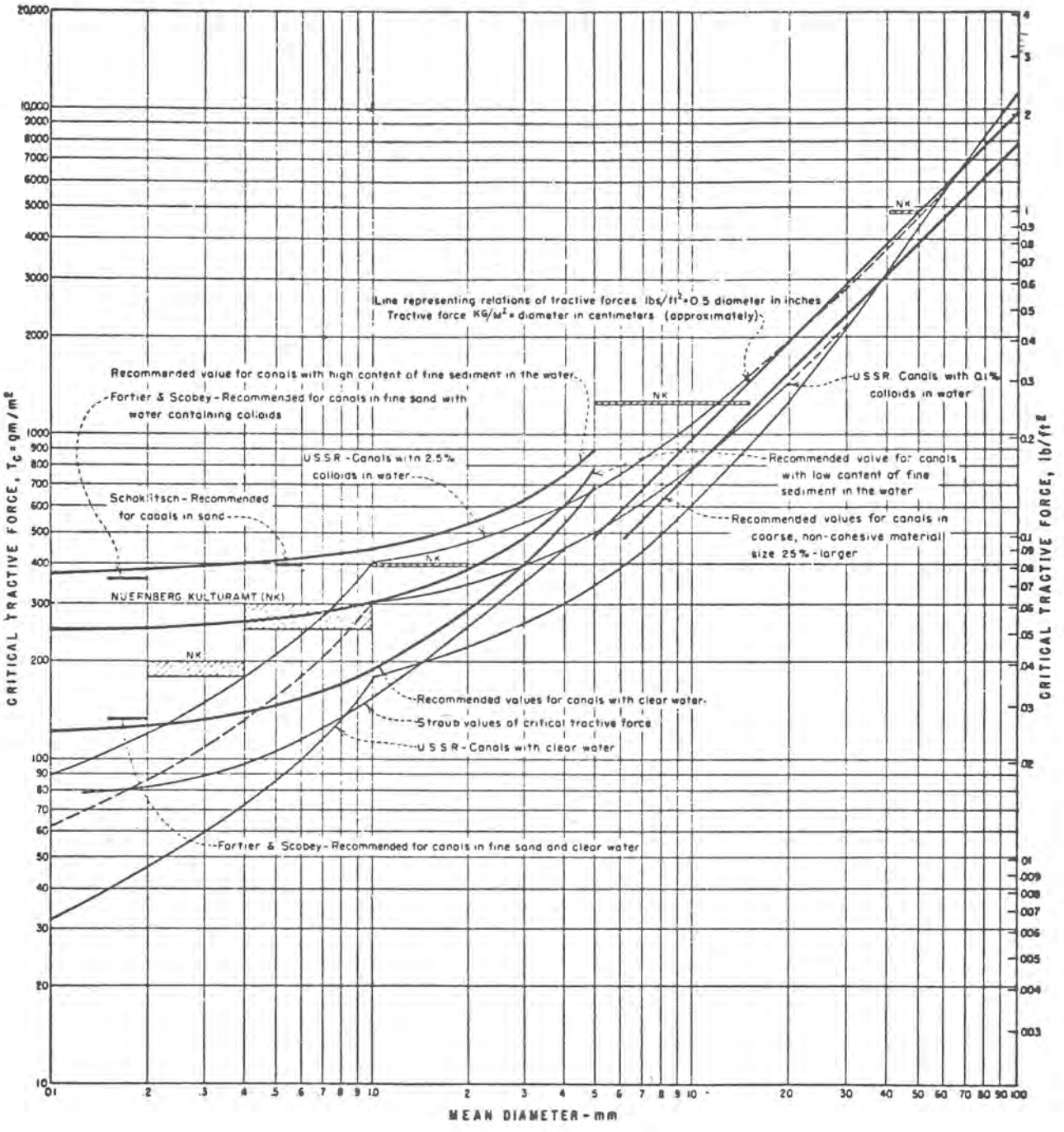

Figure 7 - Limiting tractive forces recommended for canals and observed in rivers[38]

Table 3. Comparison of Etcheverry's maximum allowable velocities and tractive forces[38]

Material	Value of Manning's n used	Velocity ft/sec	Tractive force lb/sq ft
Very light pure sand of quicksand character	0.020	0.75-1.00	0.006-0.011
Very light loose sand	.020	1.00-1.50	0.011-0.025
Coarse sand or light sandy soil	.020	1.50-2.00	0.025-0.045
Average sandy soil	.020	2.00-2.50	0.045-0.070
Sandy loam	.020	2.50-2.75	0.070-0.084
Average loam, alluvial soil, volcanic ash soil	.020	2.75-3.00	0.084-0.100
Firm loam, clay loam	.020	3.00-3.75	0.100-0.157
Stiff clay soil, ordinary gravel soil	.025	4.00-5.00	0.278-0.434
Coarse gravel, cobbles and shingles	.030	5.00-6.00	0.627-0.903
Conglomerate, cemented gravel, soft slate, tough hardpan, soft sedimentary rock	.025	6.00-8.00	0.627-1.114

Table 4. Comparison of Fortier and Scobey's limiting velocities with tractive force values--straight channels after aging[38]

Material	n	For clear water		Water transporting colloidal silts	
		Velocity ft/sec	Tractive force lb/sq ft	Velocity ft/sec	Tractive force lb/sq ft
Fine sand colloidal	0.020	1.50	0.027	2.50	0.075
Sandy loam noncolloidal	.020	1.75	.037	2.50	0.075
Silt loam noncolloidal	.020	2.00	.048	3.00	0.11
Alluvial silts noncolloidal	.020	2.00	.048	3.50	0.15
Ordinary firm loam	.020	2.50	.075	3.50	0.15
Volcanic ash	.020	2.50	.075	3.50	0.15
Stiff clay very colloidal	.025	3.75	.26	5.00	0.46
Alluvial silts colloidal	.025	3.75	.26	5.00	0.46
Shales and hardpans	.025	6.00	.67	6.00	0.67
Fine gravel	.020	2.50	.075	5.00	0.32
Graded loam to cobbles when noncolloidal	.030	3.75	.38	5.00	0.66
Graded silts to cobbles when colloidal	.030	4.00	.43	5.50	0.80
Coarse gravel noncolloidal	.025	4.00	.30	6.00	0.67
Cobbles and shingles	.035	5.00	.91	5.50	1.10

Table 5. USSR data on permissible velocities for noncohesive soils[38]

Material	Particle diameter mm	Mean velocity ft/sec
	0.005	0.49
Silt		
	0.05	0.66
Fine sand		
	0.25	0.98
Medium sand		
	1.00	1.80
Coarse sand		
	2.50	2.13
Fine gravel		
	5.00	2.62
Medium gravel		
	10.00	3.28
Coarse gravel		
	15.0	3.94
Fine pebbles		
	25.0	4.59
Medium pebbles		
	40.0	5.91
Coarse pebbles		
	75.0	7.87
Large pebbles		
	100.0	8.86
Large pebbles		
	150.0	10.83
Large pebbles		
	200.0	12.80

Table 6. USSR corrections of permissible velocities for depth--noncohesive soil[38]

Average depth							
Meters	0.30	0.60	1.00	1.50	2.00	2.50	3.00
Feet	0.98	1.97	3.28	4.92	6.56	8.20	9.84
Correction factor	0.8	0.9	1.00	1.1	1.15	1.20	1.25

Table 7. USSR limiting velocities and tractive forces in cohesive soil[38]

Compactness of bed								
Descriptive term	Loose		Fairly				Very	
Descriptive term	loose		compact		Compact		compact	
Voids ratio	2.0-1.2		1.2-0.6		0.6-0.3		0.3-0.2	
Principal cohesive material of bed	Limiting mean velocity ft/sec and limiting tractive force lb/sq ft							
	Ft/sec	Lb/sq ft	Ft/sec	Lb/sq ft	Ft/sec	Lb/sq ft	Ft/sec	Lb/sq ft
Sandy clays (sand content less than 50 percent)	1.48	0.040	2.95	0.157	4.26	0.327	5.90	0.630
Heavy clayey soils	1.31	0.031	2.79	0.141	4.10	0.305	5.58	0.563
Clays	1.15	0.024	2.62	0.124	3.94	0.281	5.41	0.530
Lean clayey soils	1.05	0.020	2.30	0.096	3.44	0.214	4.43	0.354

He presents a dimensionless Shields-type shear plot in terms of the grain Reynolds number and the probability (q) of remaining still. Gessler's approach can be used to determine the percentage of a given fraction of a soil gradation that will remain on the bed or that will move.

Critical Tractive Force for Cohesive Soils

Gibbs[34] gave tractive force values for plastic soils plotted along the A-line of the plastic index line. The data shown in his plot (figure 8) are for soil densities near 90 lb/ft^3. It is doubtful that a sufficient number of the soil properties will be known to apply the multiple correlations during the appraisal stage of the Undersea Aqueduct design. Some of the more complicated approaches and multiple correlations are discussed by Graf[37].

Critical Velocity Versus Grain Size

The critical velocity curves of Sundborg, reference 41, converted to feet per second, are shown as solid lines in figure 9. The intermediate solid line is the curve for critical velocities measured about 3 feet above the bed. (Data of Hjulstrom[42] for a critical average velocity, all fall within the bounds of Sundborg.) Kuenen critical velocity data taken from reference 41 are also plotted (dashed) for the portion outside of the bounds of the Sundborg curves and for maximum velocity for deposition. (The Hjulstrom line for sedimentation agrees almost exactly with the Kuenen deposition curve.) The regions denoted by "Erosion," "Transport," and "Sedimentation" in figure 9 are those

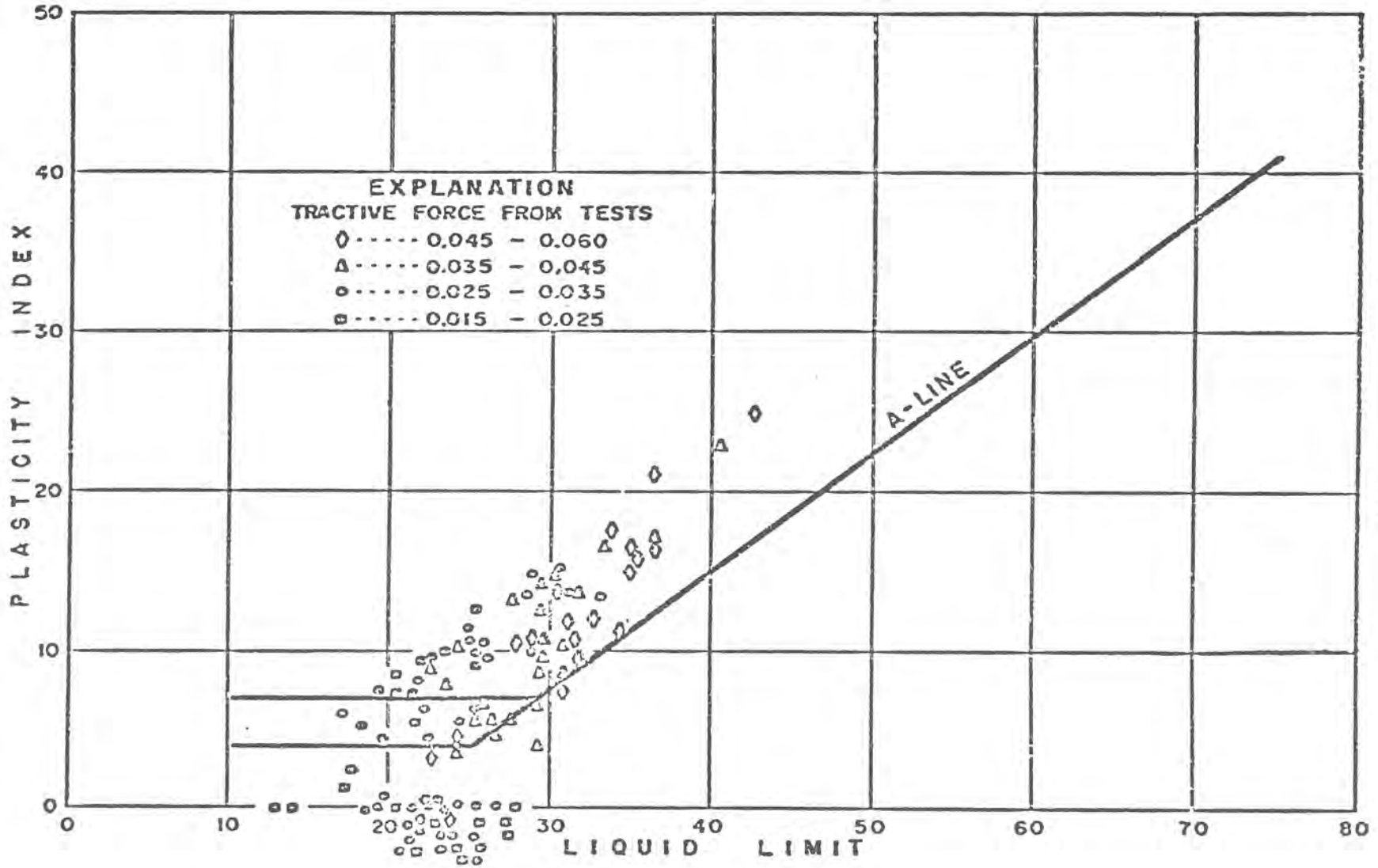

Figure 8 - Plasticity characteristics with laboratory tractive force values adjusted because of high and low density. Samples with densities below 80 PCF were raised in value and samples with densities above 100 PCF were lowered in value

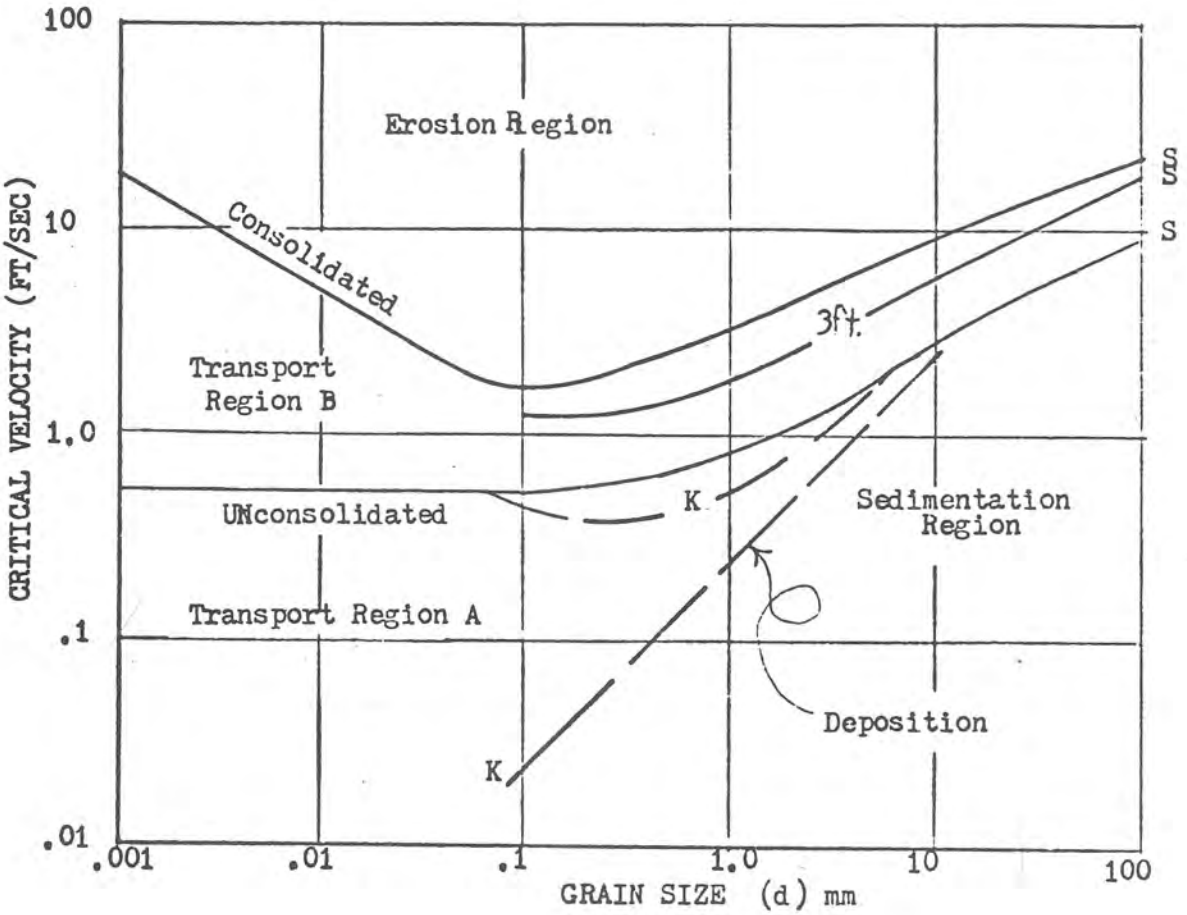

S - Sundborg
K - Kuenen

Figure 9 - Grain size and critical velocity relationships[41,42]

designated by Hjulstrom. The indication of consolidation of the fine soils is from Sundborg.

It is proper to consider the velocities along the unconsolidated line as those causing particles to be lifted from the bed and transported. In Region A between this line and the "Deposition" line, particles will remain in suspension once they are already in suspension. Region B, between the consolidated line and the unconsolidated line, shows an increasing range of variation of resistance to erosion for soils with diameters less than 0.1 mm where cohesive effects start.

LOCAL SCOUR

Background

Laursen[43] essentially stated that the fundamental characteristics of local scour are:

1. The rate of scour is the difference between the rate of sediment supply approaching the scour area, and the rate of local transport from the scour area.

2. The rate of scour will decrease as the scour hole enlarges and approaches an equilibrium shape which limits the extent of scour.

3. The limit of scour will be approached asymptotically with respect to time.

For design purposes, these statements imply that in some way flow conditions are known before and after placing the structure. These statements also imply adequate knowledge of the sediment properties for determining or computing the transport, both before construction and after placing the structure. Otherwise, model or field measurements

are required. When a structure is placed in or on the bed, flow is accelerated and the turbulence is changed around parts of the structure. Wake, trailing, and horseshoe vortexes can be produced.

Scour Trends

Blunt-nose piers have maximum scour depth upstream in the stagnation zone; sharp-nose piers have the maximum scour depth downstream. Scour tendency patterns are given in references [44,45,46,47].

Scour Depth Envelope

For design, Shen et al[44], suggest their equation be used as an upper envelope for clear water scour. Their equation is

$$d_s = 0.00073\ R^{0.619} \qquad (10)$$

where

d_s = equilibrium scour depth

R = pier Reynolds number

If there is a continuous sediment transport in the approach flow, then the value of equilibrium scour depth should also be computed from Larras'[48] equation. The smallest value of the two should be used. Larras' equation is

$$d_{se}^* = 1.42\ Kb^{0.75} \qquad (11)$$

where

K = 1 for cylindrical piers

K = 1.4 for rectangular piers aligned with flow

d_{se}^* = depth of scour

b = diameter or width of projected plane normal to flow

= D for cylinder

When there is general sediment transport in the approaching flow, dunes can travel along with the flow. Half the height of the largest expected dune should be added to the estimated equilibrium depth of scour to predict the maximum probable depth. Traveling dunes or ripples 6 feet high have been reported in the oceans[33].

Possible limitations of Shen et al's design method are that data are for freshwater, for grain sizes ranging from 0.08 to 0.68 mm and apply only to noncohesive soils.

The Reynolds number fully accounts for variations in water properties. The equilibrium depth (d_s) may not need correction for difference in submerged weight. A change of submerged weight could be considered tantamount to a change of diameter size and Shen et al[44] show data that suggest that a change of grain size causes shift along the equation line. A significant velocity will have to be defined to apply Shen et al's method to flows with wave oscillation.

Time Rate of Local Scour

Carstens[47] provides considerable evidence that all local scouring relationships due to disturbances are of the form

$$\frac{S}{L} = f\left[(N_s^2 - N_{sc}^2)^{5/2}, \frac{d}{L}, \frac{Vt}{L}\right]$$

where the symbols not previously defined are

c = (subscript) denotes critical value

S = settlement or scour depth

L = fundamental dimension of structure = D for cylinder

t = time

V = reference velocity

$N_s = V\sqrt{(\gamma_s - \gamma_f)\ gd}$

d = sediment grain size

His dimensionless plots for both a vertical or horizontal cylinder suggest an asymtotic value for the vertical cylinder (S/D) of 1.5 but at one time his (S/D) was as high as 2. The (S/D) limit of settlement for the horizontal cylinder is 1. The data for the horizontal cylinders are limited to ratios of length to diameter equal to 4.

Underflow Scour

No quantitative information was found on local scour for long cylinders supported above or on the bed. The only method outside of model studies for the pipe above the bed is to estimate, by proportioning the approach flow over and under the pipe by potential theory, the increase of velocity under the pipe, and checking for critical velocity. If the velocity is above critical, then a bed shape is assumed and the depth of scour found that will bring the velocity back to just below critical. It would probably be assumed that the slopes of the scour hole would be near the submerged angle of repose, as Carstens[47] found for scour holes. As a first approximation or for lack of data, the submerged angle of repose would be assumed to be about 30° for noncohesive sediments with mean diameters greater than 0.1 mm.

Wave oscillation and vortex trails can create pulsating forces on the bed or even produce alternating lifting of the pipe from the bed. Long reaches of a pipe partially buried or resting on the bed can be easily underscoured and left unsupported. The pipes can either settle or rupture. No suitable information was found to help compute the amount of scour depth and the required bridging strength.

Scour by Fluidization

Posey[49] describes another mode of scour occurring around oil towers having many piles and braces disturbing the flow. For long waves, pressures can be transmitted into permeable soils causing in and out flow. If this action fluidizes the soil, the soil can move out. No suggestion for predicting this scour was made.

SCOUR NEAR THE BEACH

The transport of sediment is complicated by the direction, refraction, and focusing of waves which cause long-shore currents that carry sediment along the coast, feeding gullies and canyons that carry sediment out to deeper water. Water accumulates after successive waves, causing strong rip currents that can carry large amounts of suspended sediment, cut channels through the offshore bars, and carry fines out to deeper water. Wave orbits can continue to cause sediment movement out into deeper water. Vortex ripples have been found out to a depth of 170 feet. Wind-caused upwelling or tilt of the water surface can contribute to wave backwash currents.

The backwash can be in or out of phase with mass transport of the wave. Wave steepness changes transport action; the beach can have a storm or winter profile versus a berm-type or summer profile. Tides change the still-water level and cause currents. Both profiles continually change sediment transport, and bedform characteristics of the beach.

Trask[50] defines the active zone to a water depth of less than 30 feet, whether sediment grain size decreases with depth. He defines a more or less tranquil zone to a depth greater than 60 feet where there is very little movement and sediment grain size diminishes as depth increases. In the beach zone, the pipe should be buried out to at least the 60-foot depth. Between 30 to 60 feet there is occasional movement but grain size remains nearly constant.

Scour in Cohesive Soil

No information on local scour was found for cohesive soils in consolidated, unconsolidated or ooze soils found in the ocean. The unconsolidated forms would have virtually no resistance to scour. After foundation feasibility has been established, before and after tractive force values can be used to determine whether critical velocity or critical tractive force are exceeded. If critical values are exceeded, scour cannot be predicted and scour protection such as riprap or anchoring into bedrock must be considered.

TRANSPORT CALCULATIONS

Transport calculations have been successful in predicting aggradation and degradation after placement of dams in rivers. The possibility of computing scour has been previously implied in this section. These computations[2] are time consuming and require considerable field data. They are not recommended for appraisal stage design.

SOME LIMITATIONS

Critical velocities and tractive forces should be considered as guides only. They do not always account for flow section shapes or turbulent fluctuations. Data generally were obtained from rivers or flume studies with freshwater rather than seawater. Seawater has greater density than freshwater. Therefore, sediment particles have less submerged weight. For a given velocity, the flowing water also has more force to carry the sediment and to scour. Because of these effects of water density, care should be used in applying freshwater data to seawater. The locations of velocities are not always clearly defined and the moment of initial movement is based on the decision of many different individual observers.

The results usually are expressed in terms of single grain sizes or very uniform distribution of grain sizes. Those using these data for graded soils must select some characteristic grain size (50 percent size or larger) that could be assumed to effectively hide or protect the finer sizes.

Scour

Dimensionless approaches are preferred because they are self-correcting for water properties. The Gessler function[40] is recommended for noncohesive soils because it can be applied to soils with grain distributions and can be used to predict armoring. In any case, decisions made from any scour criteria need be tempered by the engineer's experience and judgment. Much field experience concerning scour has been gained by the oil industry in the Gulf of Mexico. These data will no doubt be used for the North Sea Pipeline construction. Experience in these endeavors can be used to advantage in any future activity on the California Continental Shelf.

Bridge pier studies provide a source of local scour data but are usually presented in forms that include discharge, energy gradients, Froude number, and depth of flow. Therefore, few studies can be easily applied to the ocean bottom. This is the reason that approaches of Shen et al[44] and Carstens[47] were stressed. However, these data must be used with care when obstructions are such that turbulent eddies from their tops might increase the downstream scour.

CENTURY RISK DATA

COLLECTION OF DATA

The data in this section are essentially all the century risk data assembled by NUC contract work for the USBR. These data and the methodology for determining the century extremes and their confluences are described in more detail in NUC Technical Paper No. 353.[1]

DATA CONTENTS

Table 8 gives the lowest and highest extreme values of seawater density likely to be observed over a century for 11 localities. These include: Cape Mendocino, Noya Canyon, Bodega Bay, San Francisco, Ascension Canyon, Pt. Piedras Blancas, San Luis Obispo, Pt. Arguello, Santa Barbara, Santa Rosa Island, and San Pedro.

Table 9 shows for 8 localities the greatest extreme bottom wave orbit surge velocity likely to be observed over a century.

Table 10 presents the greatest extreme wave periods, lengths, and heights likely to be observed over a century for the same localities. The 8 localities are Crescent City, Noya Canyon, San Francisco, Pt. Conception, East of Pt. Conception, Santa Barbara, San Miguel Island, and Santa Cruz Island.

Table 11 indicates greatest extreme bottom current likely to occur during a century along the California coast.

Table 12 presents a sample of horizontal water velocity due to an extreme tsunami as predicted by solitary wave theory for various depths and latitudes.

Table 8 Lowest and highest extreme values of σ_t likely to be observed over a century.

Part A.
Latitude 40°14′ Longitude 124°25′;
Approximate location: Cape Mendocino

Confidence Bound (Probability)	Depth, m							
	Low Density				High Density			
	200	100	50	20	200	100	50	20
0.80			24.99	24.00			26.80	27.20
0.85			24.97	23.96			26.83	27.26
0.90			24.95	23.92			26.88	27.34
0.95			24.93	23.87			26.95	27.48
0.96			24.92	23.86			26.98	27.52
0.97			24.91	23.84			27.01	27.57
0.98			24.90	23.82			27.05	27.65
0.99			24.88	23.79			27.12	27.78
0.995			24.87	23.76			27.20	27.91
0.999			24.84	23.71			27.36	28.21

Part B.
Latitude 39°46′ Longitude 124°00′;
Approximate location: Noya Canyon

Confidence Bound (Probability)	Depth, m							
	Low Density				High Density			
	200	100	50	20	200	100	50	20
0.80			24.85				26.98	
0.85			24.83				27.02	
0.90			24.81				27.08	
0.95			24.78				27.18	
0.96			24.77				27.21	
0.97			24.76				27.24	
0.98			24.74				27.30	
0.99			24.72				27.39	
0.995			24.70				27.48	
0.999			24.67				27.70	

Part C.
Latitude 38°30′ Longitude 123°22′;
Approximate location: Bodega Bay

Confidence Bound (Probability)	Depth, m							
	Low Density				High Density			
	200	100	50	20	200	100	50	20
0.80			25.14	25.09			26.98	26.64
0.85			25.12	25.07			27.01	26.67
0.90			25.10	25.06			27.06	26.71
0.95			25.07	25.03			27.14	26.78
0.96			25.06	25.02			27.17	26.80
0.97			25.05	25.02			27.19	26.83
0.98			25.04	25.00			27.24	26.87
0.99			25.02	24.99			27.32	26.93
0.995			25.01	24.98			27.40	27.00
0.999			24.98	24.95			27.58	27.15

Part D.
Latitude 37°53′ Longitude 123°01′;
Approximate location: San Francisco

Confidence Bound (Probability)	Depth, m							
	Low Density				High Density			
	200	100	50	20	200	100	50	20
0.80			24.91	24.58			26.98	27.10
0.85			24.89	24.56			27.02	27.20
0.90			24.86	24.53			27.07	27.35
0.95			24.83	24.50			27.16	27.59
0.96			24.82	24.49			27.19	27.66
0.97			24.81	24.47			27.23	27.76
0.98			24.79	24.46			27.28	27.90
0.99			24.77	24.44			27.37	28.13
0.995			24.76	24.42			27.46	28.36
0.999			24.72	24.38			27.66	28.90

Table 8 Continued.

Part E.
Latitude 37°19′ Longitude 122°36′;
Approximate location: Ascension Canyon

Confidence Bound (Probability)	Depth, m							
	Low Density				High Density			
	200	100	50	20	200	100	50	20
0.80			24.90	24.24			26.94	26.79
0.85			24.87	24.21			26.98	26.84
0.90			24.85	24.18			27.03	26.91
0.95			24.81	24.14			27.13	27.01
0.96			24.81	24.13			27.16	27.05
0.97			24.79	24.12			27.19	27.09
0.98			24.78	24.10			27.25	27.16
0.99			24.76	24.08			27.34	27.26
0.995			24.74	24.06			27.42	27.37
0.999			24.71	24.02			27.63	27.62

Part F.
Latitude 35°37′ Longitude 121°16′
Approximate location: Pt. Piedras Blancas

Confidence Bound (Probability)	Depth, m							
	Low Density				High Density			
	200	100	50	20	200	100	50	20
0.80			24.93	24.74			26.81	26.61
0.85			24.91	24.72			26.84	26.64
0.90			24.89	24.70			26.88	26.69
0.95			24.86	24.67			26.96	26.77
0.96			24.85	24.66			26.98	26.79
0.97			24.84	24.65			27.01	26.82
0.98			24.83	24.64			27.05	26.87
0.99			24.81	24.62			27.12	26.94
0.995			24.80	24.61			27.19	27.02
0.999			24.77	24.58			27.35	27.19

Part G.
Latitude 35°04′ Longitude 120°52′
Approximate location: San Luis Obispo Bay

Confidence Bound (Probability)	Depth, m							
	Low Density				High Density			
	200	100	50	20	200	100	50	20
0.80		25.40	25.45			26.78	26.51	
0.85		25.39	25.43			26.81	26.53	
0.90		25.37	25.42			26.84	26.55	
0.95		25.35	25.41			26.91	26.59	
0.96		25.34	25.40			26.93	26.61	
0.97		25.33	25.40			26.96	26.63	
0.98		25.32	25.39			26.99	26.65	
0.99		25.30	25.38			27.05	26.69	
0.995		25.30	25.37			27.11	26.73	
0.999		25.27	25.36			27.25	26.83	

Part H.
Latitude 34°27′ Longitude 120°32′
Approximate location: Pt. Arguello

Confidence Bound (Probability)	Depth, m							
	Low Density				High Density			
	200	100	50	20	200	100	50	20
0.80			24.70	24.37			26.73	26.50
0.85			24.68	24.34			26.77	26.54
0.90			24.65	24.32			26.82	26.59
0.95			24.62	24.28			26.91	26.68
0.96			24.61	24.27			26.94	26.71
0.97			24.60	24.26			26.97	26.75
0.98			24.58	24.25			27.02	26.80
0.99			24.57	24.22			27.10	26.89
0.995			24.56	24.20			27.19	26.98
0.999			24.55	24.17			27.38	27.19

Table 8 Continued.

Part I.
Latitude 34°14′ Longitude 119°22′
Approximate location: Santa Barbara

Confidence Bound (Probability)	Depth, m							
	Low Density				High Density			
	200	100	50	20	200	100	50	20
0.80				24.43				26.30
0.85				24.41				26.34
0.90				24.39				26.39
0.95				24.36				26.46
0.96				24.35				26.49
0.97				24.34				26.52
0.98				24.33				26.57
0.99				24.31				26.64
0.995				24.30				26.72
0.999				24.27				26.90

Part J.
Latitude 33°52′ Longitude 120°00′
Approximate location: Santa Rosa Island

Confidence Bound (Probability)	Depth, m							
	Low Density				High Density			
	200	100	50	20	200	100	50	20
0.80		25.72	24.79	24.19		26.64	26.78	26.47
0.85		25.71	24.77	24.16		26.66	26.81	26.51
0.90		25.70	24.75	24.13		26.68	26.86	26.57
0.95		25.69	24.72	24.10		26.72	26.95	26.67
0.96		25.68	24.71	24.09		26.74	26.97	26.70
0.97		25.68	24.71	24.07		26.76	27.00	26.24
0.98		25.67	24.70	24.06		26.78	27.05	26.80
0.99		25.66	24.68	24.04		26.82	27.13	26.89
0.995		25.65	24.66	24.02		26.86	27.21	26.99
0.999		25.64	26.63	23.98		26.96	27.40	27.21

Part K.
Latitude 33°28′ Longitude 117°46′
Approximate location: San Pedro

Confidence Bound (Probability)	Depth, m							
	Low Density				High Density			
	200	100	50	20	200	100	50	20
0.80	26.13	25.30	24.65	24.11	26.73	26.76	26.54	25.95
0.85	26.13	25.29	24.63	24.09	26.74	26.79	26.57	25.99
0.90	26.12	25.27	24.61	24.07	26.76	26.83	26.63	26.03
0.95	26.11	25.25	24.58	24.04	26.79	26.89	26.71	26.11
0.96	26.11	25.24	24.57	24.04	26.80	26.91	26.74	26.14
0.97	26.10	25.23	24.56	24.03	26.81	26.93	26.77	26.17
0.98	26.10	25.23	24.55	24.01	26.82	26.96	26.82	26.21
0.99	26.09	25.21	24.53	24.01	26.85	27.02	26.89	26.29
0.995	26.09	25.20	24.52	23.98	26.88	27.08	26.97	26.36
0.999	26.08	25.18	24.49	23.95	26.94	27.21	27.16	26.53

Table 9 Greatest extreme bottom surge velocity (cm/sec) likely to be observed over a century.

Part A.
Latitude 42°00′ Longitude 125°00′
Approximate location: Crescent City

Confidence Bound (Probability)	Depth, m			
	200	100	50	20
0.80	15.0	49.1	94.3	253.9
0.85	16.2	50.9	96.6	256.5
0.90	17.8	53.4	99.8	260.0
0.95	20.4	57.6	105.1	265.7
0.96	21.3	58.9	106.8	267.6
0.97	22.5	60.6	108.9	269.8
0.98	24.1	62.9	111.9	273.1
0.99	27.0	66.8	117.0	278.5
0.995	29.8	70.7	122.0	283.5
0.999	36.6	79.7	133.5	294.9

Part B.
Latitude 39°36′ Longitude 124°30′
Approximate location: Noya Canyon

Confidence Bound (Probability)	Depth, m			
	200	100	50	20
0.80	10.2	44.4	94.8	181.7
0.85	11.0	46.3	97.4	185.7
0.90	12.2	48.9	101.0	260.6
0.95	14.3	53.2	106.9	266.3
0.96	15.0	54.6	108.8	268.1
0.97	15.9	56.4	111.3	270.4
0.98	17.3	58.9	114.7	273.6
0.99	19.7	63.1	120.5	278.9
0.995	22.2	67.4	126.2	284.1
0.999	28.4	77.3	139.6	295.9

Part C.
Latitude 37°36′ Longitude 123°30′
Approximate location: San Francisco

Confidence Bound (Probability)	Depth, m			
	200	100	50	20
0.80	9.6	46.0	101.4	261.1
0.85	10.5	48.2	104.7	264.1
0.90	11.7	51.2	109.3	268.3
0.95	13.9	56.4	116.9	275.1
0.96	14.7	58.1	119.3	277.3
0.97	15.7	60.2	122.4	280.0
0.98	17.9	63.2	126.8	283.8
0.99	19.7	68.5	134.2	290.2
0.995	22.5	73.7	141.7	296.4
0.999	29.5	86.1	159.1	310.6

Part D.
Latitude 34°22′ Longitude 120°30′
Approximate location: Pt. Conception

Confidence Bound (Probability)	Depth, m			
	200	100	50	20
0.80	13.4	38.1	73.0	152.4
0.85	14.1	39.1	74.4	154.8
0.90	15.1	40.4	76.2	158.3
0.95	16.8	42.5	79.2	241.3
0.96	17.4	43.2	80.2	242.3
0.97	18.0	44.0	81.4	243.4
0.98	19.0	45.2	83.1	245.0
0.99	20.6	47.2	86.1	247.7
0.995	22.2	49.2	89.0	250.3
0.999	25.7	53.7	95.9	256.5

Table 9 Continued.

Part E.
Latitude 34°22′ Longitude 120°05′
Approximate location: East of Pt. Conception

Confidence Bound (Probability)	Depth, m			
	200	100	50	20
0.80	14.7	34.4	63.1	129.9
0.85	15.5	35.4	64.6	132.7
0.90	16.6	36.8	66.6	136.5
0.95	18.4	39.1	70.0	224.6
0.96	19.0	39.8	71.1	225.7
0.97	19.7	40.7	72.5	227.1
0.98	20.7	42.0	74.4	229.0
0.99	22.3	44.1	77.7	232.3
0.995	23.9	46.2	81.1	235.5
0.999	27.4	51.1	88.8	242.7

Part F.
Latitude 34°17′ Longitude 119°45′
Approximate location: Santa Barbara

Confidence Bound (Probability)	Depth, m			
	200	100	50	20
0.80	8.1	26.7	52.9	111.3
0.85	8.6	27.3	53.8	112.8
0.90	9.3	28.2	54.9	114.9
0.95	10.5	29.7	56.8	118.5
0.96	10.9	30.2	57.5	119.6
0.97	11.4	30.7	58.2	121.1
0.98	12.0	31.5	59.3	123.1
0.99	13.2	32.9	61.2	126.6
0.995	14.3	34.2	63.0	129.9
0.999	16.7	37.2	67.3	138.0

Part G.
Latitude 34°10′ Longitude 120°20′
Approximate location: San Miguel Island

Confidence Bound (Probability)	Depth, m			
	200	100	50	20
0.80	9.0	30.0	59.8	125.8
0.85	9.6	30.9	60.9	128.0
0.90	10.5	32.1	62.5	130.9
0.95	12.0	34.0	65.2	135.9
0.96	12.4	34.6	66.0	137.5
0.97	13.0	35.4	67.1	139.6
0.98	13.8	36.4	68.6	142.5
0.99	15.3	38.2	71.2	147.4
0.995	16.6	40.0	73.8	152.2
0.999	19.8	44.1	79.9	239.0

Part H.
Latitude 34°05′ Longitude 119°40′
Approximate location: Santa Cruz Island

Confidence Bound (Probability)	Depth, m			
	200	100	50	20
0.80	10.9	38.3	77.2	163.2
0.85	11.6	39.3	78.7	165.9
0.90	12.5	40.7	80.6	169.6
0.95	14.1	43.1	83.9	175.7
0.96	14.6	43.8	84.9	250.7
0.97	15.3	44.7	86.3	252.2
0.98	16.2	46.0	88.2	254.2
0.99	17.8	48.3	91.4	257.6
0.995	19.5	50.5	94.6	260.8
0.999	23.3	55.5	102.2	267.8

Table 10 – Greatest extreme wave periods, lengths, and heights likely to be observed over a century.

Part A.
Latitude 40°00′ Longitude 125°00′
Approximate location: Crescent City

Confidence Bound (Probability)	Period, sec	Deep Sea Height, m	200-m Depth		100-m Depth		50-m Depth		20-m Depth	
			Length, m	Height, m	Length, m	Height, m	Length, m	Height, m	Length, m	Height, m
0.80	17.9	10.8	495	10.8	445	10.8	355	10.8	242	10.8
0.85	18.2	11.0	508	11.0	455	11.0	361	11.0	248	11.0
0.90	18.5	11.2	528	11.2	468	11.2	370	11.2	257	11.2
0.95	19.1	11.7	559	11.7	490	11.7	385	11.7	272	11.7
0.96	19.3	11.8	569	11.8	497	11.8	389	11.8	277	11.8
0.97	19.6	12.0	582	12.0	506	12.0	395	12.0	283	12.0
0.98	19.9	12.2	601	12.2	519	12.2	404	12.2	292	12.2
0.99	20.5	12.6	632	12.6	540	12.6	418	12.6	308	12.6
0.995	21.9	13.0	663	13.0	561	13.0	432	13.0	323	13.0
0.999	22.4	14.0	736	14.0	609	14.0	464	14.0	361	14.0

Part B.
Latitude 39°36′ Longitude 124°30′
Approximate location: Noya Canyon

Confidence Bound (Probability)	Period, sec	Deep Sea Height, m	200-m Depth		100-m Depth		50-m Depth		20-m Depth	
			Length, m	Height, m	Length, m	Height, m	Length, m	Height, m	Length, m	Height, m
0.80	16.1	11.5	405	11.5	378	11.5	311	11.5	214	11.5
0.85	16.3	11.8	415	11.8	386	11.8	316	11.8	217	11.8
0.90	16.6	12.1	428	12.1	396	12.1	323	12.1	223	12.1
0.95	17.0	12.6	450	12.6	412	12.6	334	12.6	234	12.6
0.96	17.2	12.8	457	12.8	418	12.8	337	12.8	238	12.8
0.97	17.4	13.0	466	13.0	424	13.0	342	13.0	243	13.0
0.98	17.6	13.3	479	13.3	434	13.3	348	13.3	249	13.3
0.99	18.0	13.8	502	13.8	450	13.8	358	13.8	261	13.8
0.995	18.5	14.2	524	14.2	466	14.2	369	14.2	273	14.2
0.999	19.5	15.4	577	15.4	502	15.4	393	15.4	300	15.4

Part C.
Latitude 37°36′ Longitude 123°30′
Approximate location: San Francisco

Confidence Bound (Probability)	Period, sec	Deep Sea Height, m	200-m Depth		100-m Depth		50-m Depth		20-m Depth	
			Length, m	Height, m	Length, m	Height, m	Length, m	Height, m	Length, m	Height, m
0.80	15.7	12.6	384	12.6	362	12.6	300	12.6	208	12.6
0.85	15.9	12.9	393	12.9	369	12.9	305	12.9	213	12.9
0.90	16.1	13.4	405	13.4	378	13.4	311	13.4	220	13.4
0.95	16.6	14.0	425	14.0	394	14.0	321	14.0	232	14.0
0.96	16.7	14.2	432	14.2	399	14.2	325	14.2	235	14.2
0.97	16.8	14.5	440	14.5	405	14.5	329	14.5	240	14.5
0.98	17.1	14.9	452	14.9	414	14.9	335	14.9	247	14.9
0.99	17.5	15.6	473	15.6	429	15.6	345	15.6	258	15.6
0.995	17.9	16.2	494	16.2	444	16.2	354	16.2	270	16.2
0.999	18.8	17.8	542	17.8	479	17.8	377	17.8	298	17.8

Table 10 – Continued.

Part D.
Latitude 34°22′ Longitude 120°30′
Approximate location: Pt. Conception

Confidence Bound (Probability)	Period, sec	Deep Sea Height, m	200-m Depth		100-m Depth		50-m Depth		20-m Depth	
			Length, m	Height, m	Length, m	Height, m	Length, m	Height, m	Length, m	Height, m
0.80	18.5	8.8	527	8.5	468	8.0	370	8.2	249	9.4
0.85	18.8	8.8	540	8.6	477	8.1	376	8.3	253	9.6
0.90	19.1	8.9	560	8.6	491	8.2	385	8.4	258	9.8
0.95	19.8	9.1	592	8.7	513	8.3	400	8.7	268	14.9
0.96	19.9	9.2	602	8.8	520	8.4	404	8.7	273	15.0
0.97	20.2	9.2	615	8.8	528	8.4	410	8.8	278	15.2
0.98	20.5	9.3	634	8.9	541	8.5	418	9.0	286	15.5
0.99	21.1	9.5	664	9.0	562	8.7	432	9.2	299	15.9
0.995	21.7	9.6	696	9.1	582	8.8	446	9.4	313	16.3
0.999	23.0	10.0	768	9.3	630	9.2	478	9.9	346	17.3

Part E.
Latitude 34°22′ Longitude 120°05′
Approximate location: East of Pt. Conception

Confidence Bound (Probability)	Period, sec	Deep Sea Height, m	200-m Depth		100-m Depth		50-m Depth		20-m Depth	
			Length, m	Height, m	Length, m	Height, m	Length, m	Height, m	Length, m	Height, m
0.80	20.7	7.0	644	6.7	548	6.4	423	6.8	281	7.9
0.85	21.2	7.1	667	6.7	563	6.5	433	6.9	287	8.1
0.90	21.7	7.2	698	6.8	584	6.6	447	7.0	296	8.3
0.95	22.7	7.4	751	6.9	619	6.8	470	7.3	313	13.7
0.96	23.0	7.4	767	6.9	630	6.8	478	7.4	319	13.8
0.97	23.4	7.5	789	6.9	644	6.9	487	7.5	328	14.0
0.98	24.0	7.6	818	7.0	663	7.0	500	7.6	341	14.3
0.99	24.9	7.7	868	7.1	696	7.2	522	7.9	362	14.8
0.995	25.9	7.9	918	7.2	729	7.4	544	8.2	383	15.3
0.999	28.1	8.3	1031	7.6	804	7.9	595	8.8	435	16.4

Part F.
Latitude 34°17′ Longitude 119°45′
Approximate location: Santa Barbara

Confidence Bound (Probability)	Period, sec	Deep Sea Height, m	200-m Depth		100-m Depth		50-m Depth		20-m Depth	
			Length, m	Height, m	Length, m	Height, m	Length, m	Height, m	Length, m	Height, m
0.80	17.4	6.6	470	6.5	427	6.1	343	6.2	233	7.0
0.85	17.7	6.7	483	6.5	437	6.1	350	6.2	237	7.1
0.90	18.0	6.7	501	6.6	449	6.2	358	6.3	242	7.2
0.95	18.6	6.8	530	6.6	470	6.2	371	6.4	250	7.3
0.96	18.8	6.8	539	6.6	477	6.3	376	6.4	253	7.4
0.97	19.0	6.9	551	6.6	485	6.3	381	6.5	256	7.5
0.98	19.3	6.9	568	6.7	497	6.3	389	6.6	261	7.6
0.99	19.9	7.0	598	6.7	517	6.4	402	6.7	269	7.8
0.995	20.4	7.1	627	6.8	536	6.5	415	6.8	276	8.0
0.999	21.7	7.3	694	6.9	581	6.7	445	7.1	295	8.2

Table 10 – Continued.

Part G.
Latitude 34°10′ Longitude 120°20′
Approximate location: San Miguel Island

Confidence Bound (Probability)	Period, sec	Deep Sea Height, m	200-m Depth		100-m Depth		50-m Depth		20-m Depth	
			Length, m	Height, m	Length, m	Height, m	Length, m	Height, m	Length, m	Height, m
0.80	17.4	7.5	466	7.4	425	6.9	342	7.0	232	7.9
0.85	17.6	7.6	479	7.4	434	7.0	348	7.0	236	8.0
0.90	18.0	7.7	497	7.5	447	7.0	356	7.2	241	8.2
0.95	18.5	7.8	527	7.6	468	7.2	370	7.3	249	8.4
0.96	18.7	7.9	536	7.6	474	7.2	374	7.4	252	8.5
0.97	18.9	7.9	548	7.7	483	7.3	380	7.5	255	8.6
0.98	19.3	8.0	565	7.7	495	7.3	388	7.6	260	8.8
0.99	19.8	8.2	595	7.8	515	7.5	401	7.8	268	9.0
0.995	20.4	8.3	624	7.9	534	7.6	414	8.0	276	9.3
0.999	21.6	8.7	692	8.2	580	8.0	444	8.4	303	15.0

Part H.
Latitude 34°05′ Longitude 119°40′
Approximate location: Santa Cruz Island

Confidence Bound (Probability)	Period, sec	Deep Sea Height, m	200-m Depth		100-m Depth		50-m Depth		20-m Depth	
			Length, m	Height, m	Length, m	Height, m	Length, m	Height, m	Length, m	Height, m
0.80	17.0	9.8	449	9.7	412	9.1	333	9.1	227	10.3
0.85	17.2	9.9	460	9.8	419	9.2	338	9.2	230	10.4
0.90	17.5	10.1	473	9.9	430	9.3	345	9.4	234	10.6
0.95	18.0	10.3	497	10.0	447	9.4	356	9.6	241	11.0
0.96	18.1	10.4	505	10.1	452	9.5	360	9.7	243	15.6
0.97	18.3	10.4	515	10.2	459	9.6	364	9.8	247	15.8
0.98	18.6	10.6	529	10.3	469	9.7	371	9.9	253	16.1
0.99	19.0	10.8	552	10.4	485	9.9	382	10.2	264	16.5
0.995	19.5	11.0	576	10.6	502	10.0	392	10.4	275	17.0
0.999	20.5	11.5	631	10.9	539	10.5	417	11.0	300	18.0

Table 11 Greatest extreme bottom current particle velocity (cm/sec) likely to be observed over a century along the California coast.

Confidence Bound (Probability)	Depth, m			
	200	100	50	20
0.80	336.6	328.9	249.2	279.9
0.85	341.4	333.5	254.0	284.8
0.90	347.9	339.8	260.5	291.5
0.95	358.7	350.3	271.3	302.7
0.96	362.2	353.7	274.8	306.3
0.97	366.6	357.9	279.1	310.8
0.98	372.8	363.9	285.3	317.2
0.99	383.3	374.1	295.8	328.0
0.995	393.8	384.3	306.3	338.8
0.999	418.1	407.8	330.5	363.9

Table 12 A sample of horizontal water particle velocity (cm/sec) caused by an extreme tsunami as predicted by solitary wave theory for six depths at ten latitudes.

Latitude, deg	Depth, m					
	200	150	100	75	50	20
42	32.78	40.64	55.13	86.36	92.71	184.31
41	30.43	37.75	51.17	63.50	86.06	171.11
40	28.09	34.85	47.24	58.61	79.44	157.95
39	25.75	31.95	43.30	53.73	72.82	144.78
38	23.41	29.04	39.36	48.84	66.20	131.62
37	21.07	26.14	35.43	43.96	59.58	118.46
36	18.72	23.23	31.49	39.07	52.96	105.50
35	16.38	20.33	29.31	34.19	46.34	92.13
34	14.04	17.43	23.62	29.31	39.72	78.97
33	11.70	14.52	19.68	24.42	33.10	65.81

CONSTRUCTION DATA

COLLECTION OF DATA

This section contains most of the construction risk data collected by NUC contract work for the USBR. These data and their implications in terms of actually constructing the Aqueduct are discussed further in NUC Technical Paper No. 353[1].

DATA CONTENTS

Table 13 presents averages and standard deviations of periods, lengths, and amplitudes for surface waves off the California coast for winter and summer at various latitudes for the 20, 50, 100, and 200-meter bathymetry contours.

Figure 10 is a series of drawings.

Parts A, B, C, D, E, and F - Ocean density off the California coast at 0, 50, and 200-meter depths for both winter and summer.

Parts G and H - Surface wave amplitudes for both winter and summer.

Parts I and J - Bottom wave orbit surge velocity for both winter and summer.

Parts K and L - Surface currents velocity for both winter and summer.

Part M - Bottom current velocity.

Parts N and O - Light transmittance.

Table 13 Averages and standard deviations of periods, lengths, and amplitudes for surface waves off the California coast.*

Season	Location		Depth, m	Period, sec	Length, m	Amplitude, m
	Latitude, deg	Longitude, deg				
Winter	42.00	125.00	20	12.41 (6.37)	157.8 (91.2)	1.96 (1.69)
			50	12.41 (6.37)	214.1 (147.9)	1.91 (1.64)
			100	12.41 (6.37)	243.0 (208.8)	2.00 (1.72)
			200	12.41 (6.37)	253.8 (285.3)	2.04 (1.76)
Summer	42.00	125.00	20	11.99 (2.80)	151.6 (42.8)	1.10 (0.91)
			50	11.99 (2.80)	203.9 (72.8)	1.07 (0.86)
			100	11.99 (2.80)	228.8 (98.3)	1.11 (0.89)
			200	11.99 (2.80)	236.0 (110.1)	1.14 (0.92)
Winter	39.60	124.50	20	12.29 (2.82)	156.3 (42.9)	2.13 (1.72)
			50	12.29 (2.82)	211.7 (73.1)	2.08 (1.67)
			100	12.29 (2.82)	239.1 (99.8)	2.17 (1.75)
			200	12.29 (2.82)	247.4 (113.0)	2.21 (1.98)
Summer	39.60	124.50	20	12.31 (2.84)	156.6 (43.2)	1.07 (0.89)
			50	12.31 (2.84)	212.3 (73.6)	1.03 (0.83)
			100	12.31 (2.84)	240.0 (100.4)	1.07 (0.87)
			200	12.31 (2.84)	248.5 (113.9)	1.10 (0.90)
Winter	37.00	123.50	20	12.41 (2.98)	158.0 (45.3)	1.93 (1.59)
			50	12.41 (2.98)	214.7 (77.1)	1.88 (1.54)
			100	12.41 (2.98)	243.8 (105.2)	1.96 (1.61)
			200	12.41 (2.98)	253.2 (119.7)	2.00 (1.65)
	37.60	123.50	20	12.31 (2.92)	156.6 (44.5)	0.97 (0.73)
			50	12.31 (2.92)	212.4 (75.7)	0.94 (0.69)
			100	12.31 (2.92)	240.5 (103.0)	0.98 (0.71)
			200	12.31 (2.92)	249.3 (116.8)	1.00 (0.74)
Winter	36.37	121.56	20	13.47 (2.04)	174.4 (31.0)	1.27 (0.84)
			50	13.47 (2.04)	242.8 (53.1)	1.27 (0.84)
			100	13.47 (2.04)	279.5 (73.2)	1.27 (0.84)
			200	13.47 (2.04)	289.0 (82.1)	1.27 (0.84)
Winter	36.37	121.52	20	13.50 (2.03)	174.9 (30.8)	2.01 (1.07)
			50	13.50 (2.03)	243.7 (52.7)	2.01 (1.07)
			100	13.50 (2.03)	280.7 (72.7)	2.01 (1.07)
			200	13.50 (2.03)	290.3 (81.5)	2.01 (1.07)
Winter	35.50	122.00	20	12.71 (3.15)	162.6 (47.8)	1.49 (1.20)
			50	12.71 (3.15)	222.7 (80.9)	1.43 (1.14)
			100	12.71 (3.15)	255.2 (110.8)	1.56 (1.31)
			200	12.71 (3.15)	266.6 (127.2)	1.62 (1.35)
Summer	35.50	122.00	20	12.49 (3.30)	159.1 (49.9)	0.88 (0.62)
			50	12.49 (3.30)	216.8 (84.3)	0.79 (0.60)
			100	12.49 (3.30)	247.8 (115.1)	0.94 (0.64)
			200	12.49 (3.30)	259.0 (132.3)	0.96 (0.67)
Winter	34.50	123.50	20	12.67 (3.07)	161.9 (46.7)	1.44 (0.97)
			50	12.67 (3.07)	221.3 (79.4)	1.39 (0.91)
			100	12.67 (3.07)	253.0 (109.4)	1.49 (0.95)
			200	12.67 (3.07)	264.0 (125.9)	1.48 (0.99)
Summer	34.50	123.50	20	12.40 (2.77)	158.1 (42.1)	1.33 (1.26)
			50	12.40 (2.77)	214.7 (21.9)	1.30 (1.25)
			100	12.40 (2.77)	242.9 (98.2)	1.35 (1.28)
			200	12.40 (2.77)	251.4 (111.3)	1.38 (1.30)

Table 13 Continued.

Season	Location		Depth, m	Period, sec	Length, m	Amplitude, m
	Latitude, deg	Longitude, deg				
Winter	34.22	120.30	20	9.46 (2.83)	111.9 (44.8)	1.18 (0.52)
			50	9.46 (2.83)	139.9 (71.4)	1.18 (0.52)
			100	9.46 (2.83)	149.9 (87.3)	1.18 (0.52)
			200	9.46 (2.83)	151.9 (92.4)	1.18 (0.52)
Summer	34.23	120.22	20	9.82 (0.40)	118.7 (6.5)	1.31 (0.63)
			50	9.82 (0.40)	146.8 (10.6)	1.31 (0.63)
			100	9.82 (0.40)	150.6 (12.0)	1.31 (0.63)
			200	9.82 (0.40)	150.6 (12.0)	1.31 (0.63)
Winter	34.21	120.18	20	9.77 (0.44)	118.0 (7.0)	2.42 (0.94)
			50	9.77 (0.44)	145.5 (11.4)	2.42 (0.94)
			100	9.77 (0.44)	149.1 (13.0)	2.42 (0.94)
			200	9.77 (0.44)	149.1 (13.0)	2.42 (0.94)
Summer	34.21	120.18	20	9.67 (0.48)	116.3 (17.8)	1.90 (0.76)
			50	9.67 (0.48)	142.9 (12.6)	1.90 (0.76)
			100	9.67 (0.48)	146.1 (14.3)	1.90 (0.76)
			200	9.67 (0.48)	146.1 (14.3)	1.90 (0.76)
Winter	34.21	120.17	20	10.21 (0.42)	124.9 (6.5)	2.27 (0.98)
			50	10.21 (0.42)	157.2 (11.2)	2.27 (0.98)
			100	10.21 (0.42)	162.8 (13.6)	2.27 (0.98)
			200	10.21 (0.42)	162.8 (13.6)	2.27 (0.98)
Winter	34.23	120.17	20	10.69 (0.84)	132.5 (13.1)	2.30 (1.15)
			50	10.69 (0.84)	170.2 (22.4)	2.30 (1.15)
			100	10.69 (0.84)	179.2 (27.9)	2.30 (1.15)
			200	10.69 (0.84)	179.4 (28.2)	2.30 (1.15)
Summer	34.23	120.17	20	10.32 (0.79)	126.7 (12.3)	1.64 (0.67)
			50	10.32 (0.79)	160.3 (21.1)	1.64 (0.67)
			100	10.32 (0.79)	167.1 (26.4)	1.64 (0.67)
			200	10.32 (0.79)	167.3 (27.7)	1.64 (0.67)
Winter	34.22	120.05	20	9.32 (2.79)	109.9 (43.8)	0.94 (0.39)
			50	9.32 (2.79)	136.7 (69.5)	0.94 (0.39)
			100	9.32 (2.79)	145.8 (84.7)	0.94 (0.39)
			200	9.32 (2.79)	147.6 (89.2)	0.94 (0.39)
Winter	34.20	120.00	20	12.94 (3.05)	166.0 (46.2)	1.38 (0.95)
			50	12.94 (3.05)	228.3 (78.8)	1.38 (0.95)
			100	12.94 (3.05)	262.3 (109.2)	1.38 (0.95)
			200	12.94 (3.05)	274.4 (126.3)	1.38 (0.95)
Summer	34.20	120.00	20	12.29 (2.69)	156.4 (40.6)	0.99 (0.55)
			50	12.29 (2.69)	211.5 (69.5)	0.99 (0.55)
			100	12.29 (2.69)	238.0 (96.5)	0.99 (0.55)
			200	12.29 (2.69)	246.0 (110.8)	0.99 (0.55)
Winter	34.10	120.20	20	9.90 (2.68)	119.0 (42.6)	1.39 (0.58)
			50	9.90 (2.68)	151.6 (66.8)	1.39 (0.58)
			100	9.90 (2.68)	162.6 (79.7)	1.39 (0.58)
			200	9.90 (2.68)	163.9 (82.2)	1.39 (0.58)
Winter	34.17	119.45	20	10.26 (3.00)	124.7 (47.2)	1.06 (0.41)
			50	10.26 (3.00)	161.3 (74.5)	1.06 (0.41)
			100	10.26 (3.00)	175.4 (91.4)	1.06 (0.41)
			200	10.26 (3.00)	178.1 (97.3)	1.06 (0.41)

Table 13 Continued.

Season	Location		Depth, m	Period, sec	Length, m	Amplitude, m
	Latitude, deg	Longitude, deg				
Winter	34.05	119.40	20	10.12 (2.45)	122.7 (38.7)	1.36 (0.44)
			50	10.12 (2.45)	156.5 (61.6)	1.36 (0.44)
			100	10.12 (2.45)	167.4 (74.9)	1.36 (0.44)
			200	10.12 (2.45)	168.9 (78.1)	1.36 (0.44)
Winter	33.50	119.50	20	12.80 (3.18)	163.8 (48.1)	1.30 (0.77)
			50	12.80 (3.18)	224.7 (81.9)	1.30 (0.77)
			100	12.80 (3.18)	259.7 (113.1)	1.30 (0.77)
			200	12.80 (3.18)	270.0 (130.9)	1.30 (0.77)
Summer	33.50	119.50	20	12.34 (2.93)	157.0 (44.5)	0.92 (0.50)
			50	12.34 (2.93)	212.8 (75.8)	0.92 (0.50)
			100	12.34 (2.93)	240.8 (104.6)	0.92 (0.50)
			200	12.34 (2.93)	250.0 (120.2)	0.92 (0.50)

*Standard deviations are in parentheses.

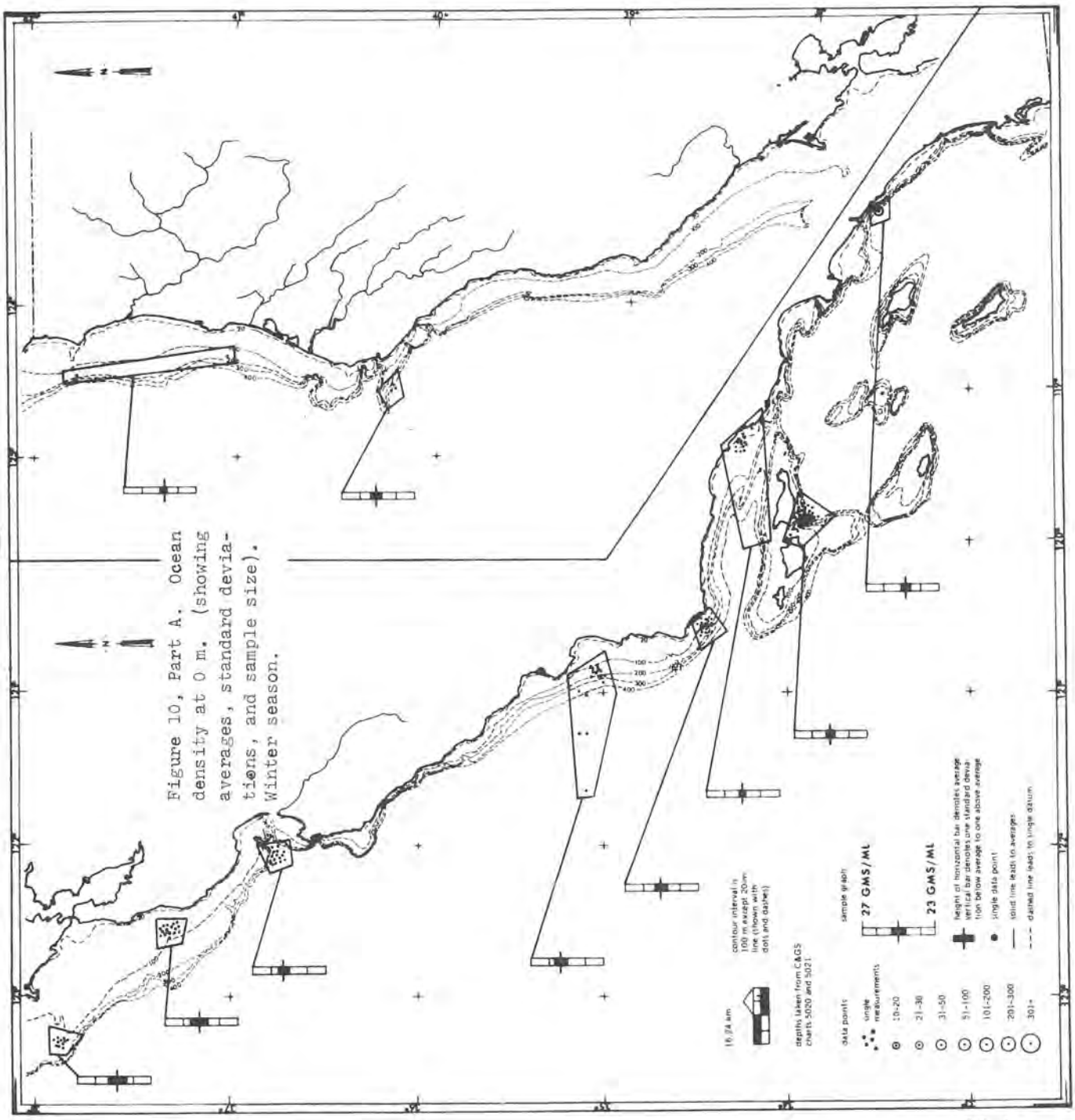

Figure 10, Part A. Ocean density at 0 m. (showing averages, standard deviations, and sample size). Winter season.

10-A

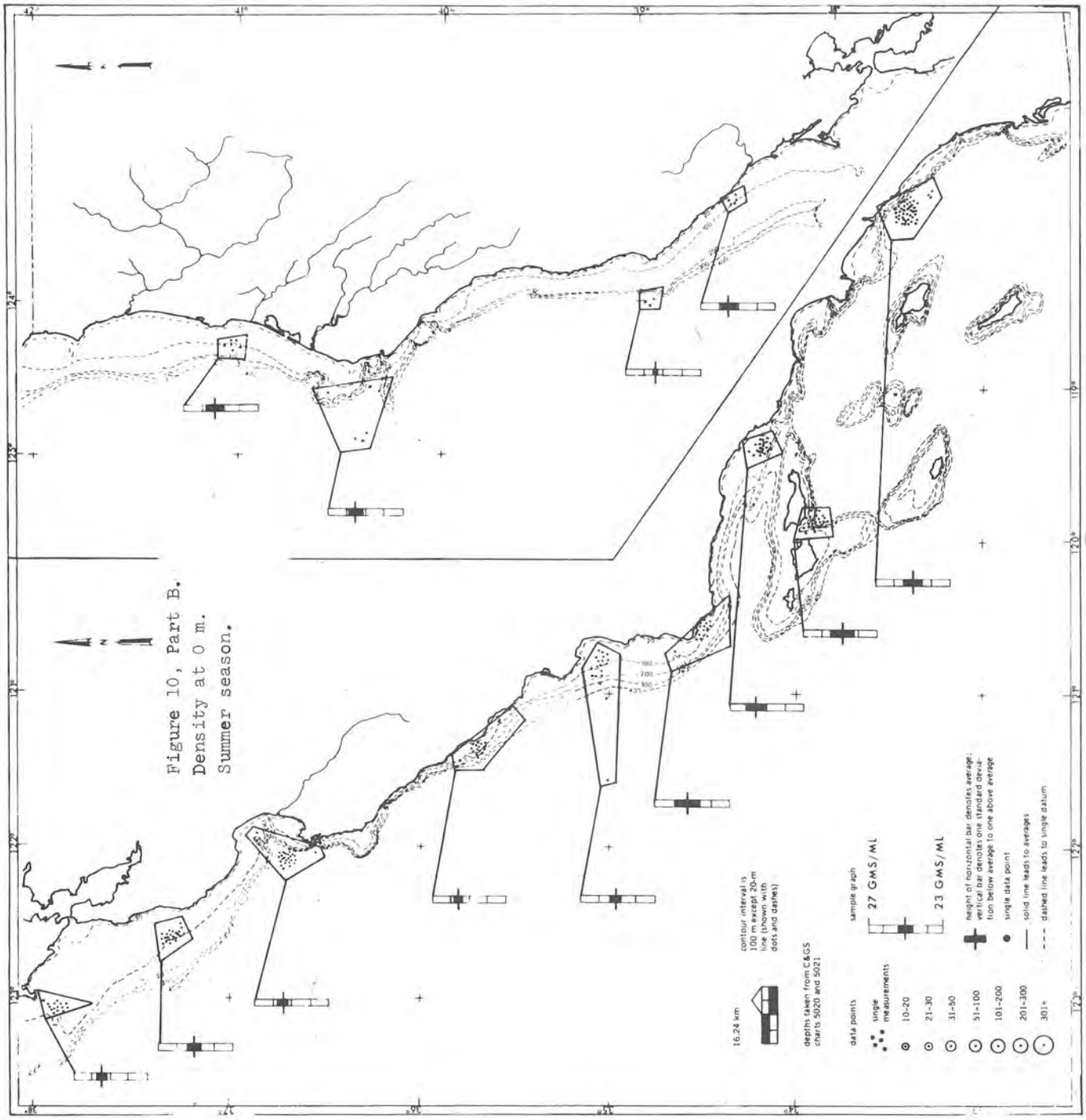

Figure 10, Part B.
Density at 0 m.
Summer season.

10-B

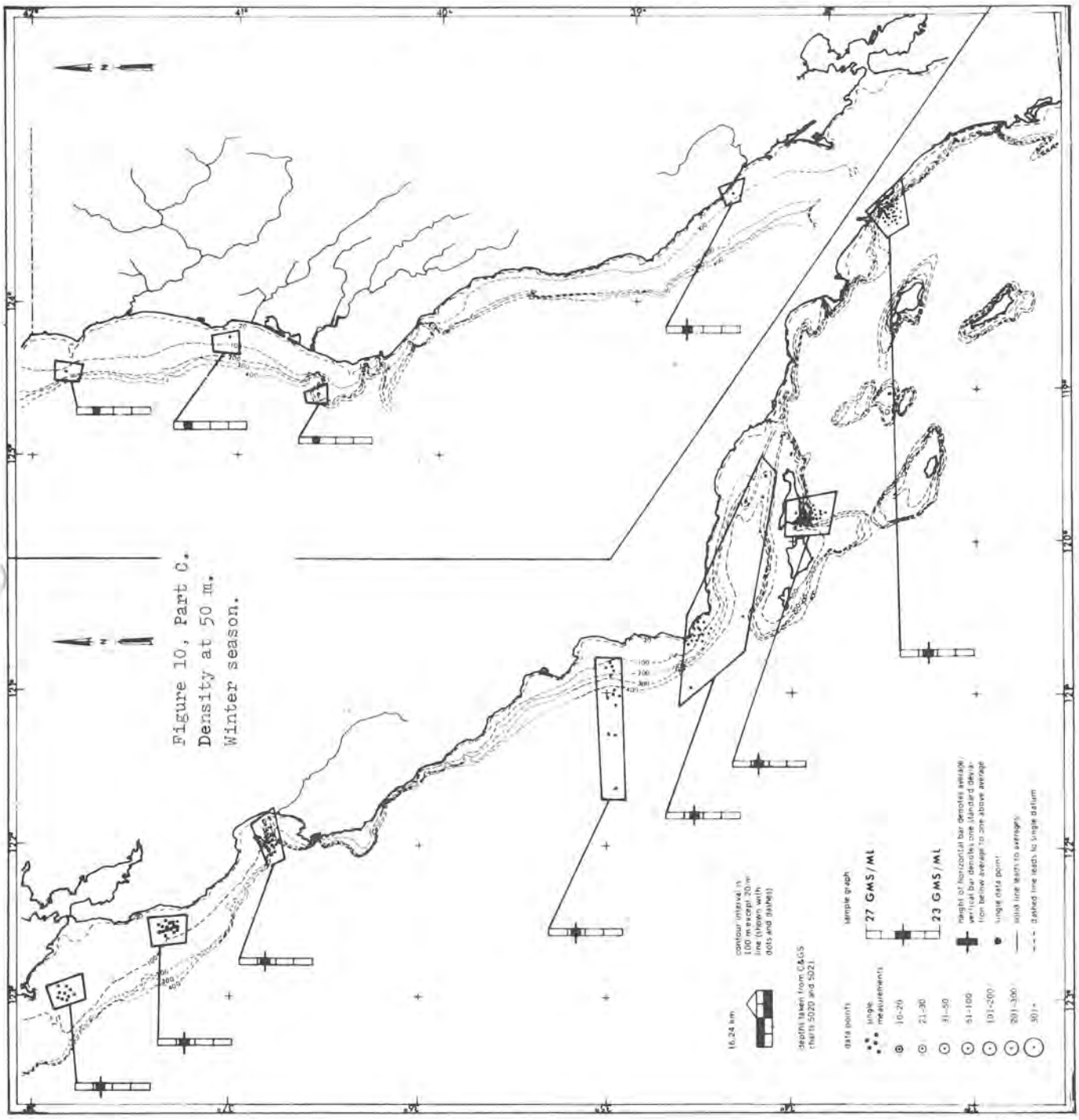
Figure 10, Part C.
Density at 50 m.
Winter season.
10-C

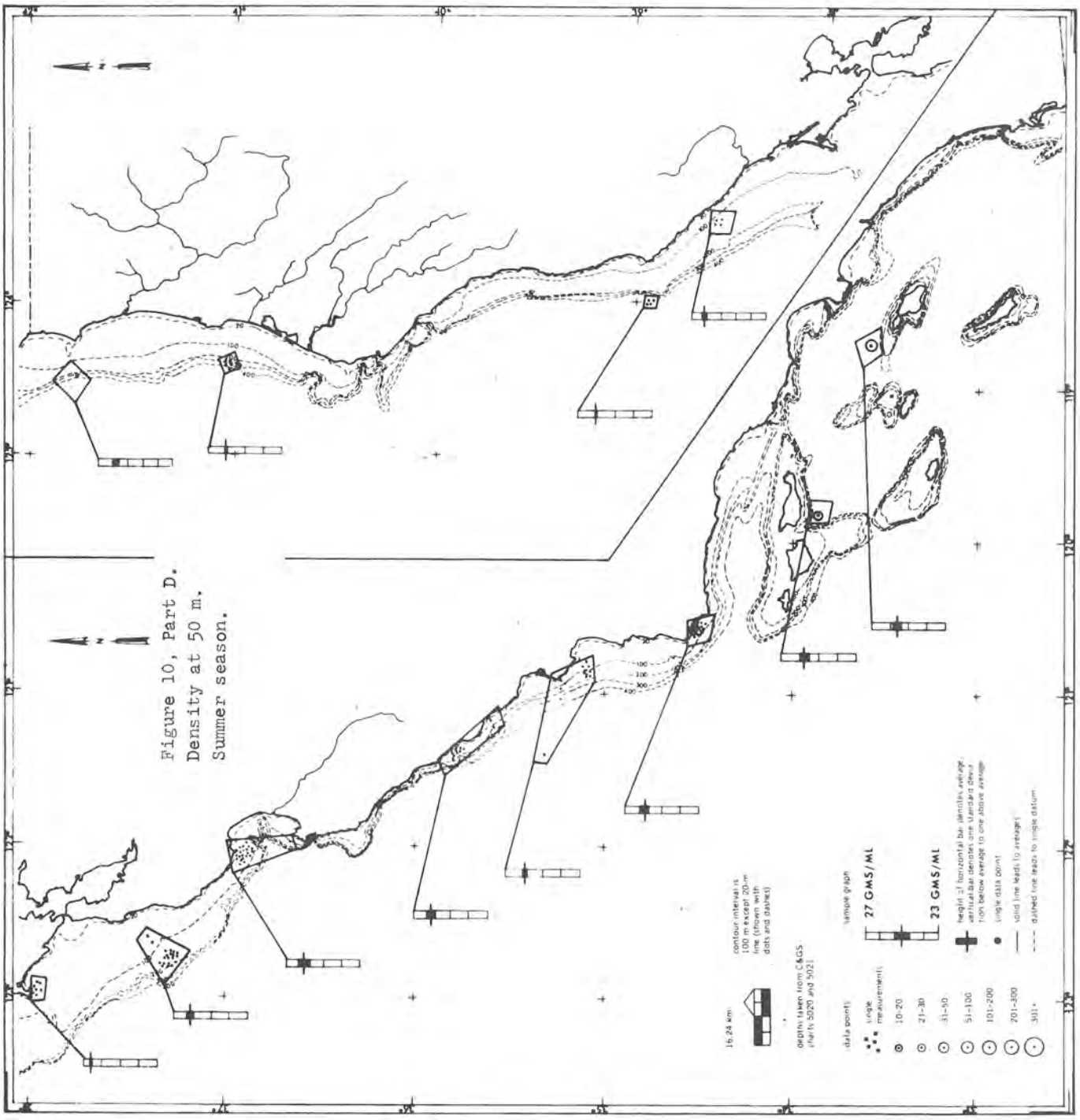
Figure 10, Part D.
Density at 50 m.
Summer season.
27 GMS/ML
23 GMS/ML

10-D

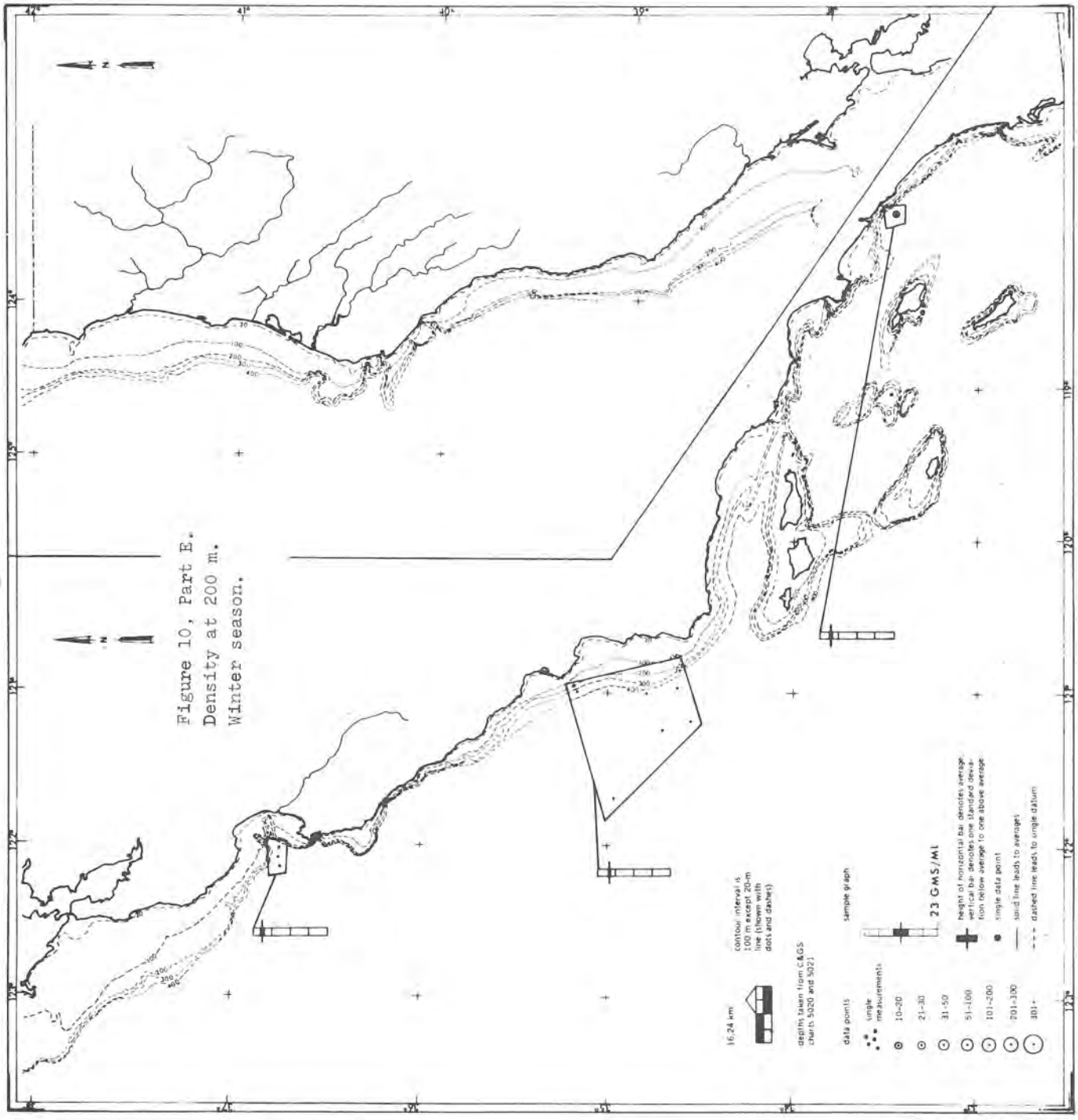
Figure 10, Part E.
Density at 200 m.
Winter season.
16.24 km
contour interval is 100 m except 20-m line (shown with dots and dashes)
depths taken from C&GS charts 5020 and 5021
data points
single measurements
10-20
21-30
31-50
51-100
101-200
201-300
301+
sample graph
23 GMS/MI
height of horizontal bar denotes average
vertical bar denotes one standard deviation below average to one above average
single data point
solid line leads to averages
dashed line leads to single datum

10-E

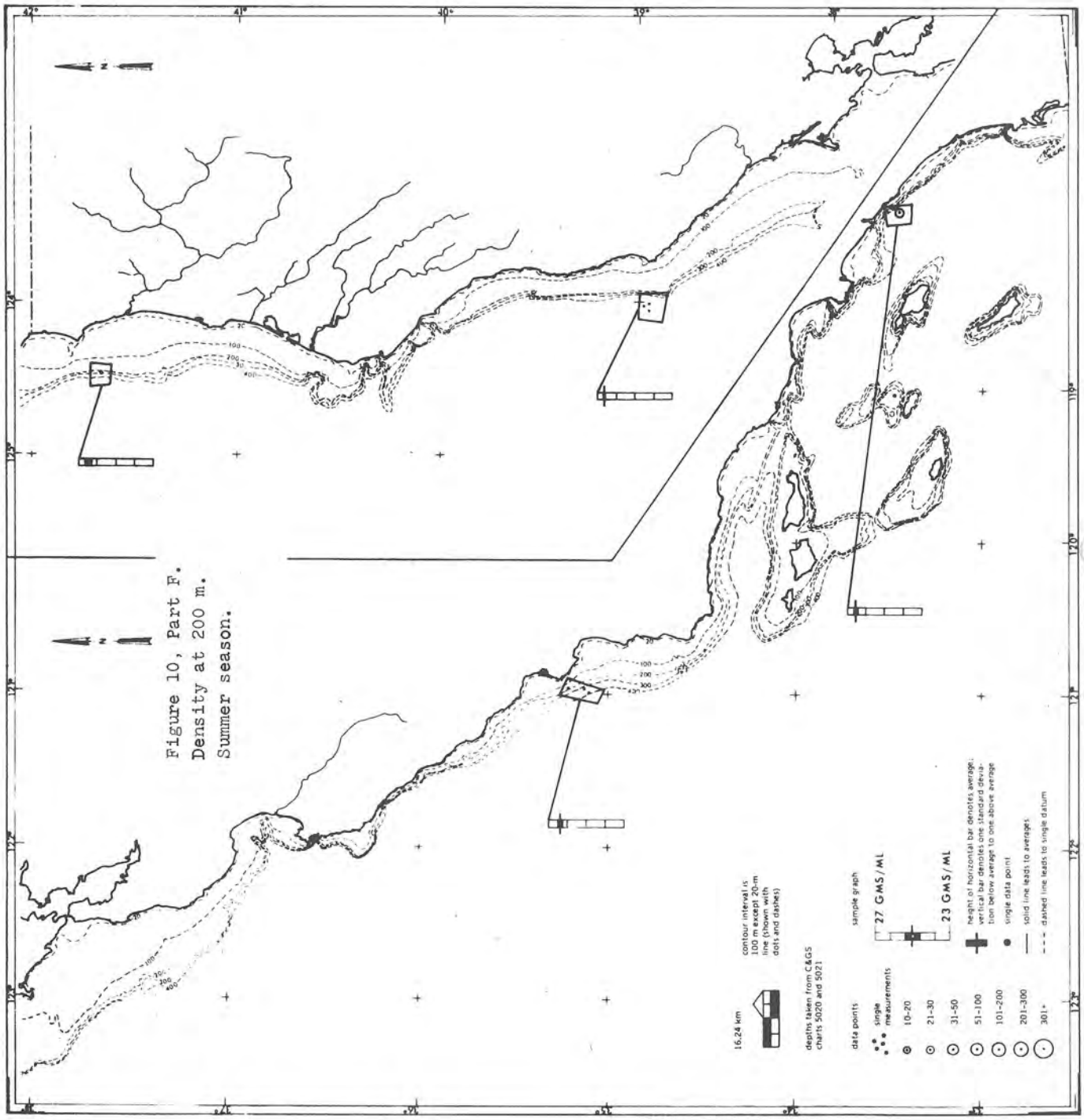
Figure 10, Part F.
Density at 200 m.
Summer season.
16.24 km
contour interval is 100 m except 20-m line (shown with dots and dashes)
depths taken from C&GS charts 5020 and 5021
data points
single measurements
10-20
21-30
31-50
51-100
101-200
201-300
301+
sample graph
27 GMS/ML
23 GMS/ML
height of horizontal bar denotes average; vertical bar denotes one standard deviation below average to one above average
single data point
solid line leads to average
dashed line leads to single datum

10-F

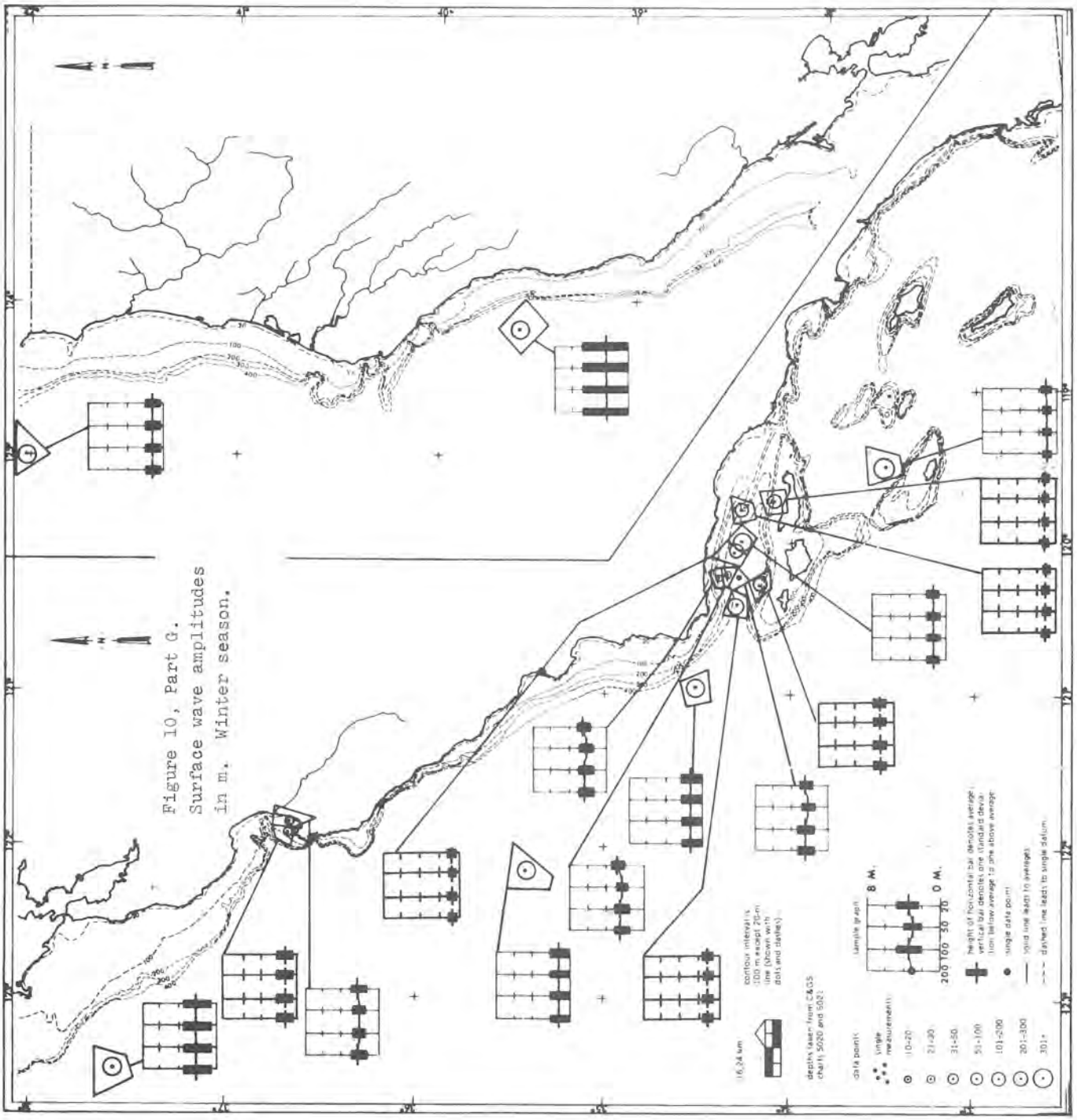

Figure 10, Part G.
Surface wave amplitudes
in m. Winter season.

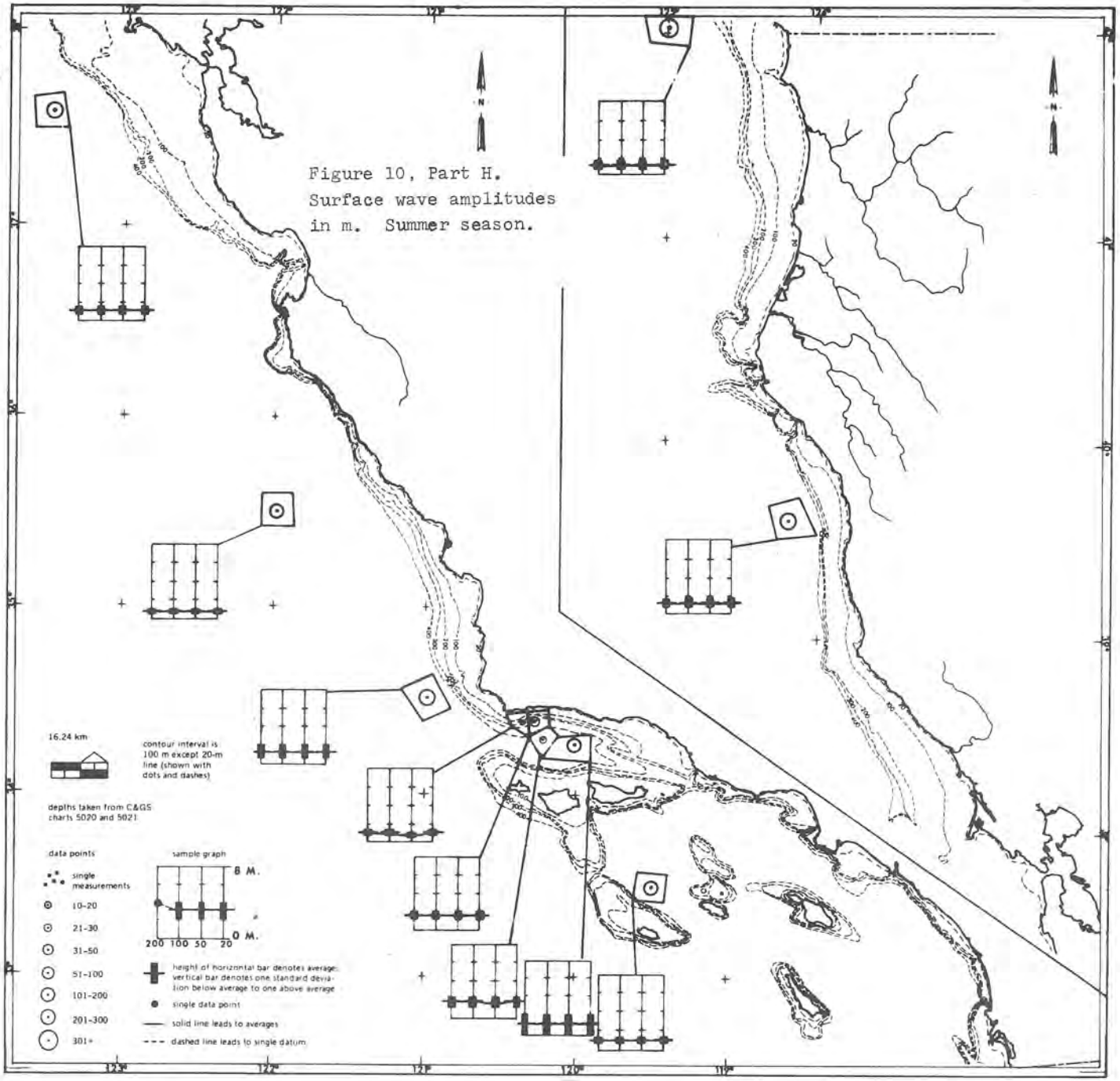

Figure 10, Part H.
Surface wave amplitudes in m. Summer season.

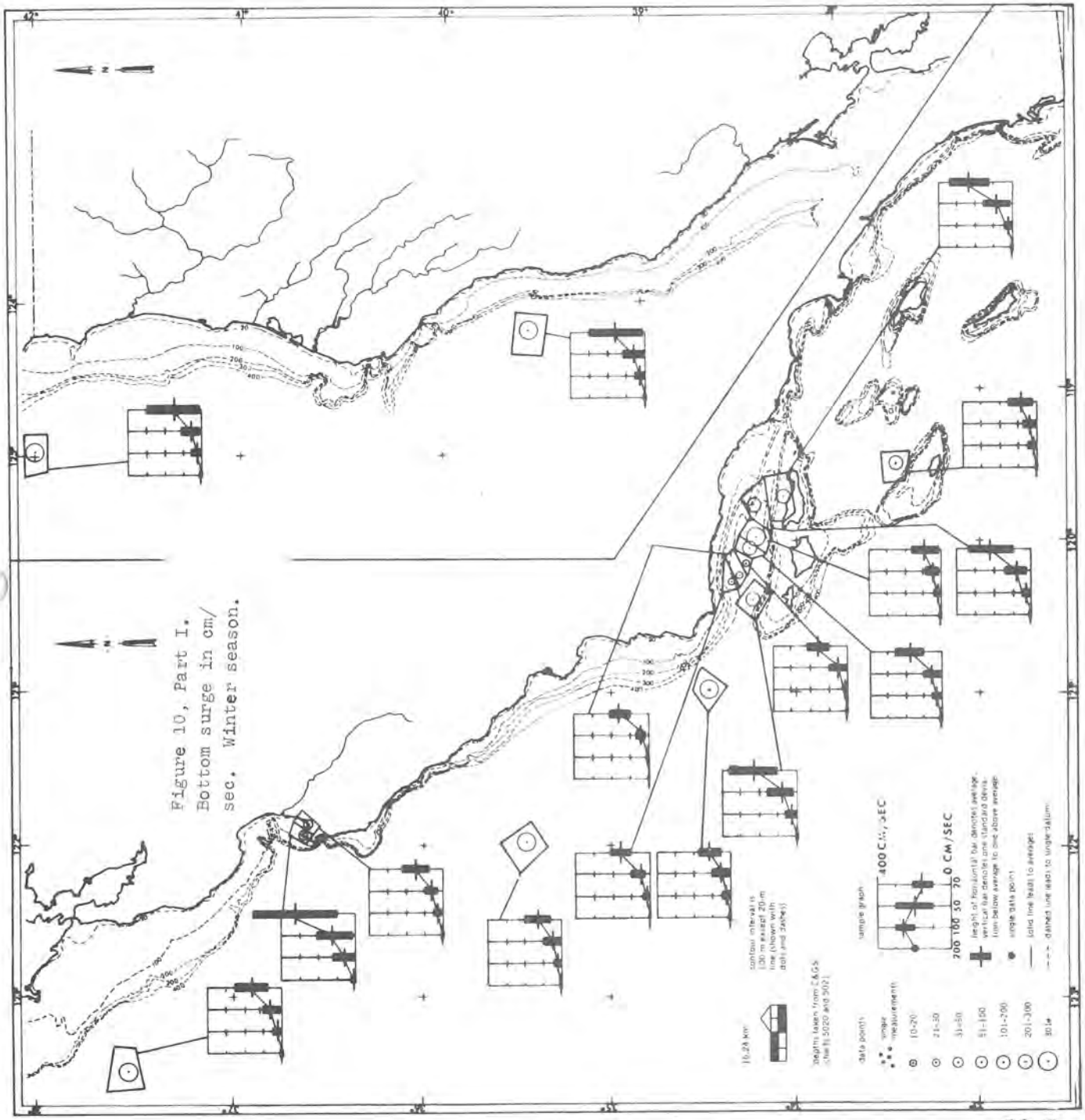

Figure 10, Part I.
Bottom surge in cm/
sec. Winter season.

10-I

Figure 10, Part J. Bottom surge in cm/sec. Summer season.

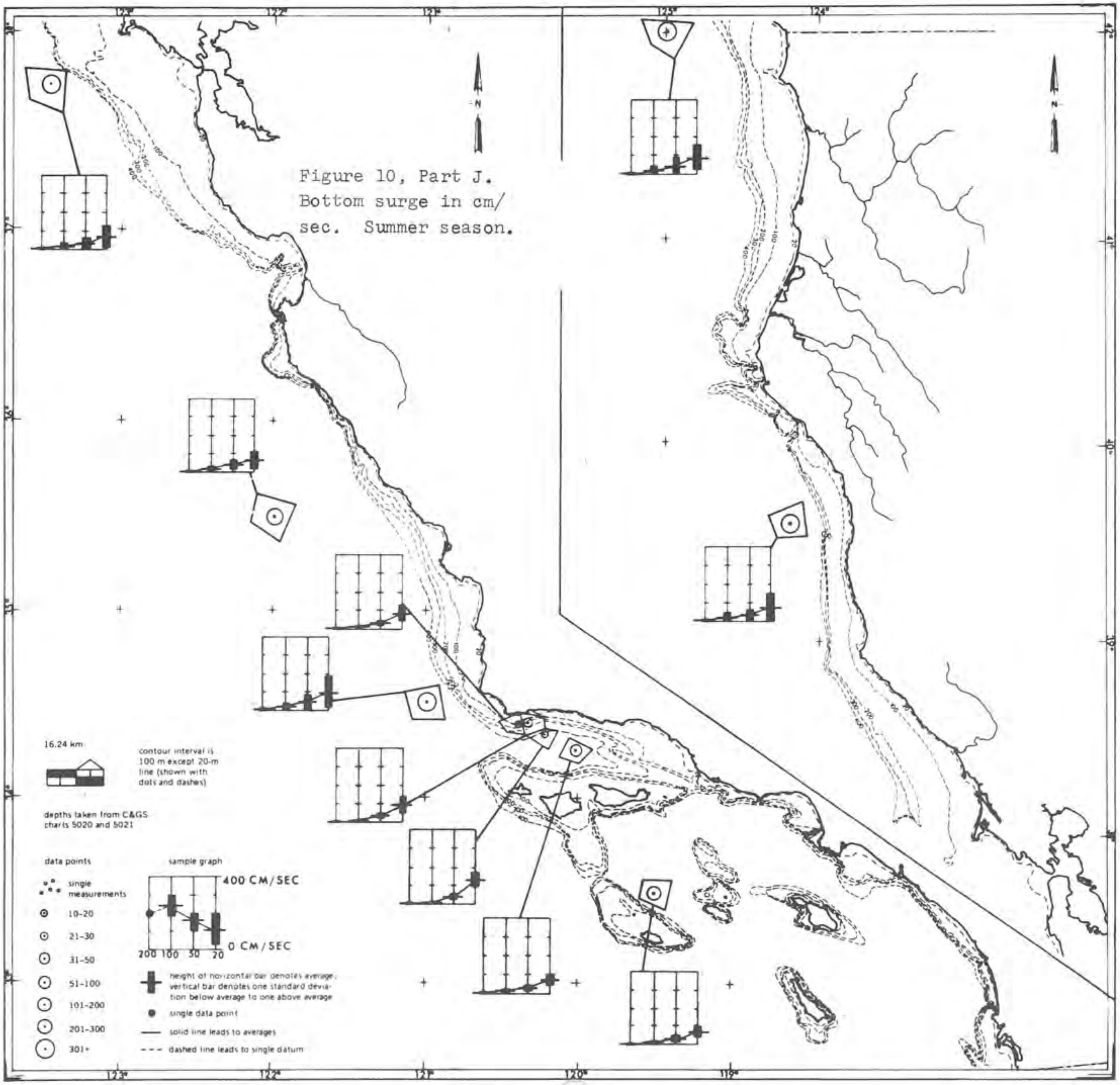

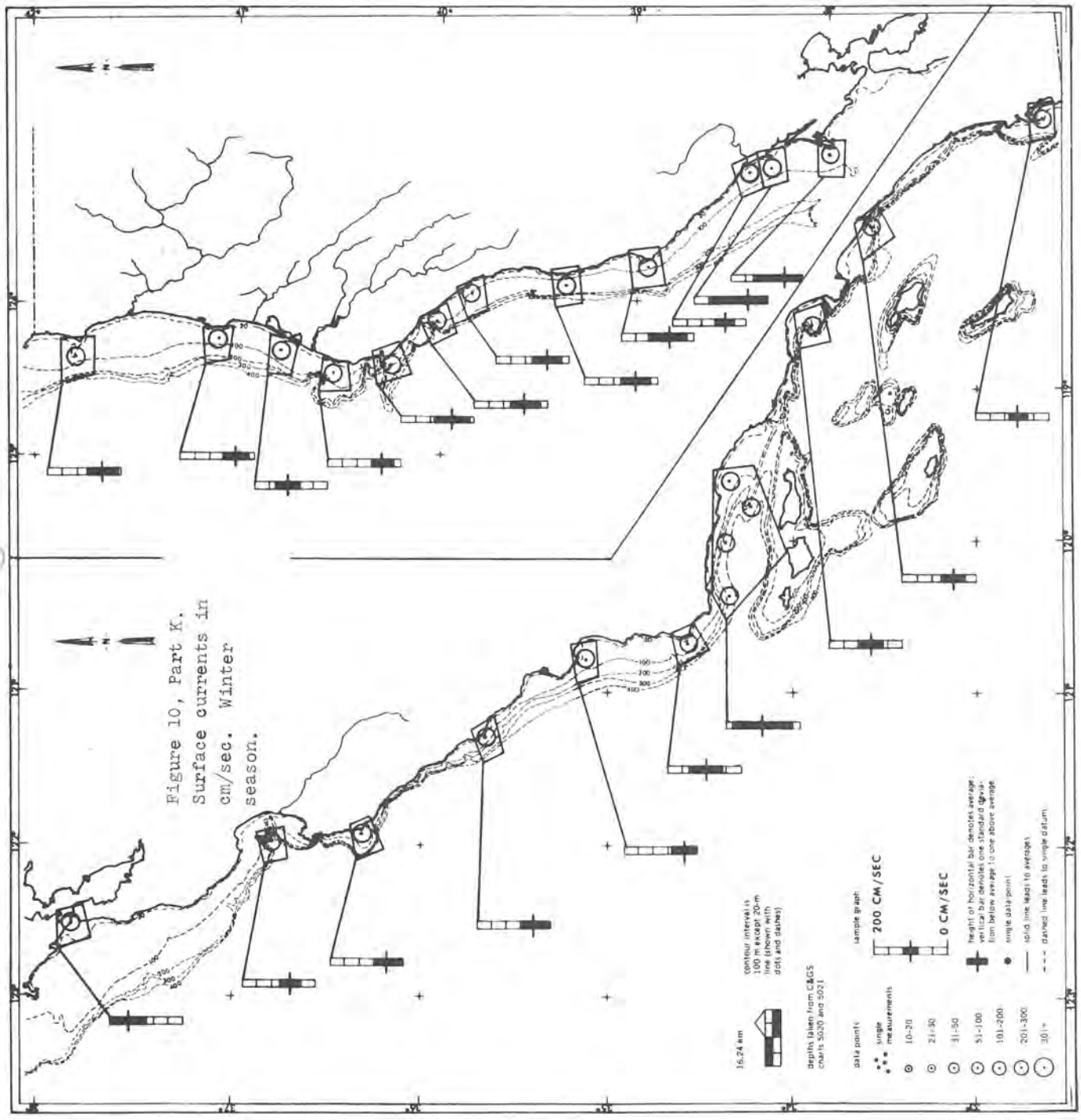

Figure 10, Part K.
Surface currents in cm/sec. Winter season.

10-K

Figure 10, Part L.
Surface currents in
cm/sec. Summer season.

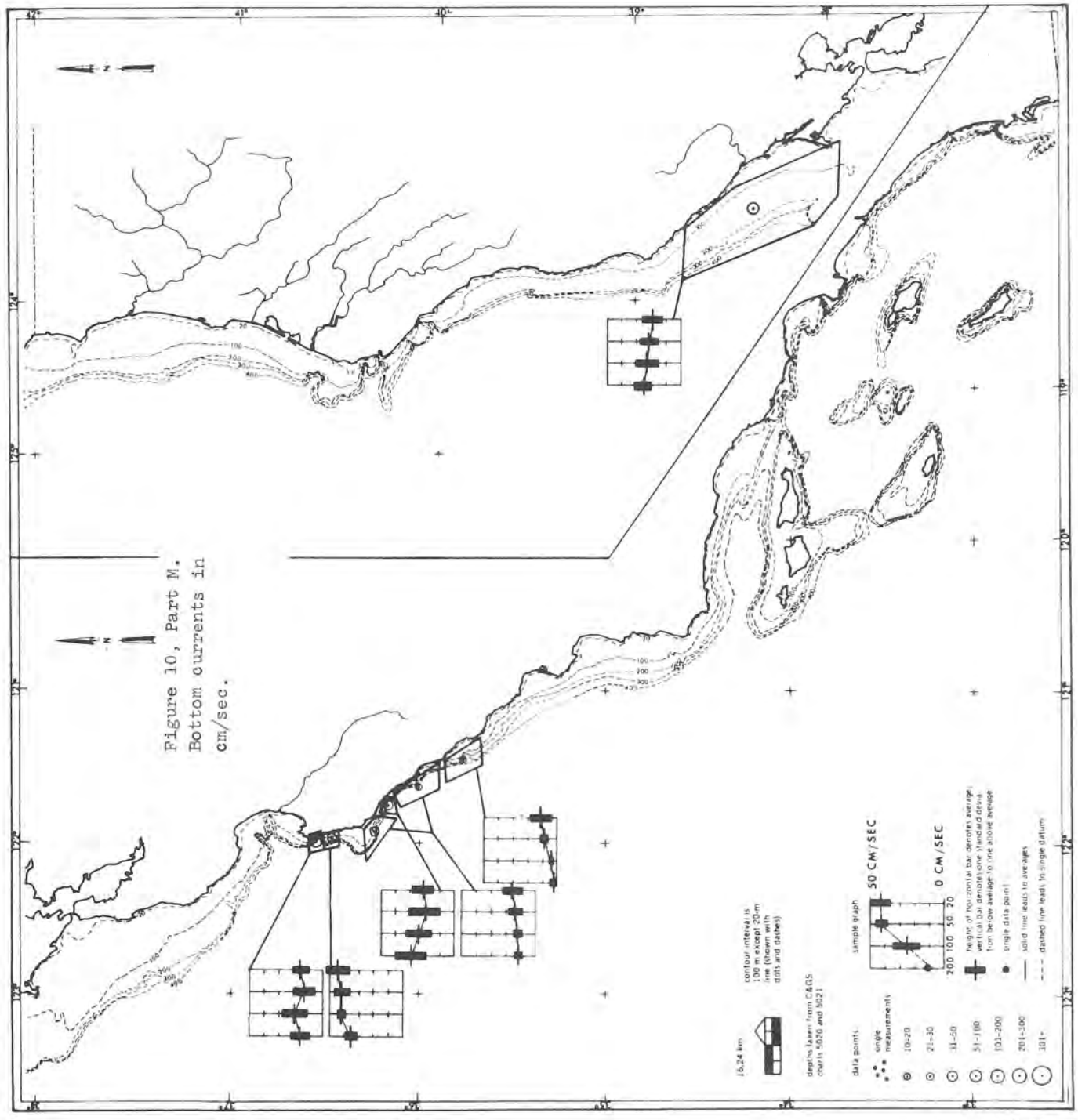
Figure 10, Part M.
Bottom currents in
cm/sec.
16.24 km
contour interval is
100 m except 20-m
line (shown with
dots and dashes)
depths taken from C&GS
charts 5020 and 5021
data points
single
measurement
10-20
21-30
31-50
51-100
101-200
201-300
301+
sample graph
50 CM/SEC
0 CM/SEC
200 100 50 20
height of horizontal bar denotes average;
vertical bar denotes one standard deviation
from below average to one above average
single data point
solid line leads to averages
dashed line leads to single datum

10-M

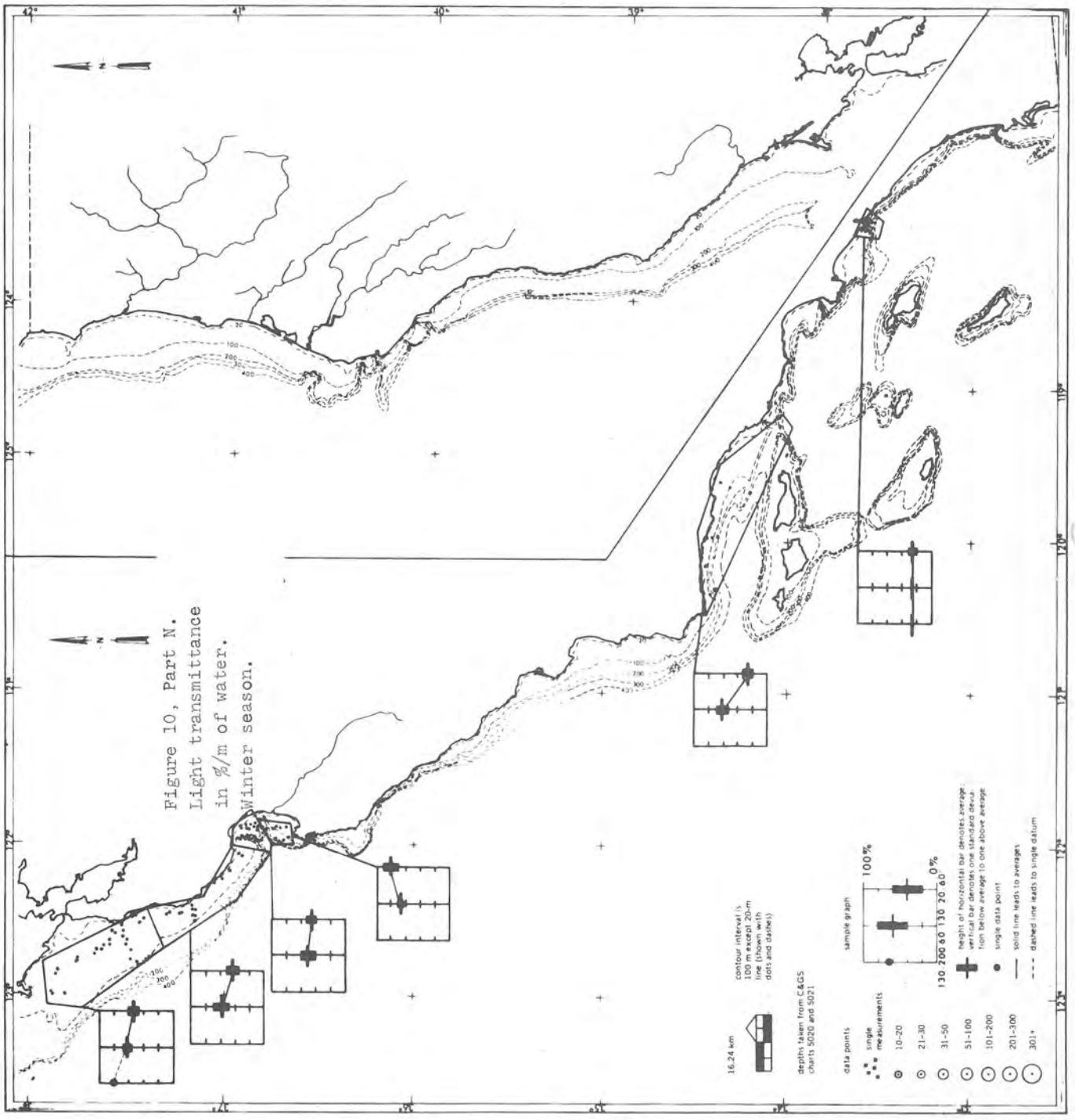

Figure 10, Part N.
Light transmittance
in %/m of water.
Winter season.

10-N

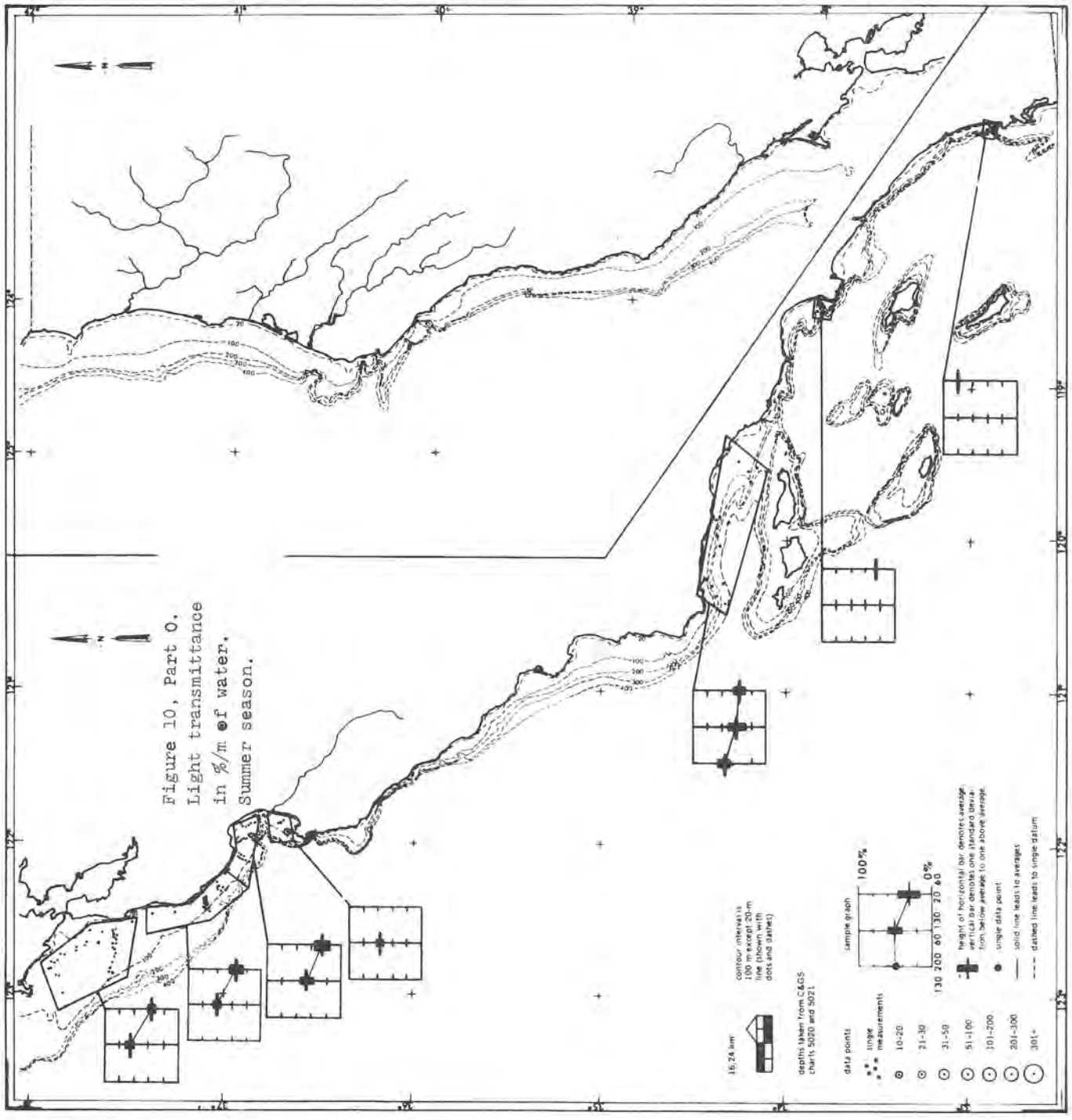

Figure 10, Part O.
Light transmittance
in %/m of water.
Summer season.

10-0

RESEARCH AND DATA NEEDS

Although the hydrodynamic studies are adequate for the appraisal planning stage, it was apparent to all investigators involved that there is still much uncertainty in regard to assessing hydrodynamic loads and scouring conditions for the Aqueduct. The extremely large conduit size severely limits the scaling of most of the model studies that have been done. Flow dynamics, structural response, and the soil environment near the Aqueduct are not explicitly defined, but are known only in approximate and general terms. Thus engineers are required to make design and estimate costs with the possibility of overdesign or underdesign. Much further research and advance of technology are required for more precise cost estimates suitable for planning beyond the appraisal stage. During the hydrodynamic studies, these research and data needs were determined.

WAVES

Prior to actual construction or any further planning beyond the appraisal stage for the Aqueduct, it is imperative that the maximum wave forces acting on the Aqueduct be known to an acceptable degree of confidence. The collection of wave data such as wave height (H), wave length (L), period (T), and accompanying water motion beneath the waves, comprise a very limited sample of data that are difficult to obtain. Maximum wave conditions which may occur for a 100-year time period off the California coast can only be estimated on a probabilistic basis.

The wave data should be used to determine whether the Airy theory or some other wave theory better defines the water motion. Accurate wave dimensions are needed when applying a wave theory. The variables wave height (H) and length (L) are usually used, but crest length--which is measured perpendicular to the wave length--could produce more critical dynamic loads along the Aqueduct than waves with indefinitely long crests. Model studies can assist in gaining knowledge for design of the Aqueduct. Accurate wave data will be essential in programming and verifying these hydraulic model studies. Onsite tests with full-scale pipe sections and anchor blocks should help. In some cases, onsite testing may be the only recourse.

LIFT, DRAG, AND OSCILLATORY FORCES

Empirical relationships have been developed for computing hydrodynamic forces acting on a circular cylinder. Numerous small model and field tests have been made to determine values of coefficients used in these relationships. However, hydrodynamic forces that act on a cylinder are unsteady and thus many test results show a wide scatter of coefficient values. Further hydraulic model and full-scale onsite tests, with carefully devised instrumentation, should be made to study and measure the magnitude and unsteadiness of the forces. Both kinds of these tests should also be used to obtain coefficients values for high Reynolds numbers and for flow configurations which have not been extensively tested.

Most data on hydrodynamic forces are for fixed bluff bodies and are not appropriate to structures that can respond to the flow. Studies made on cylinders, or other shapes, without permitting structural movement, limit the understanding of dynamic forces. The studies made with rigid bodies represent only the case where natural structural frequencies are much greater than dynamic flow frequencies.

Investigations should be extended to large cylinders one-third to one-half the diameter of the Aqueduct to confirm drag, lift, and inertia coefficients, and vortex shedding frequencies determined from small models. Flexible cylinder suspensions should be used to provide close simulation of free structure movement. Both perpendicular and angled flows should be studied as applied to the suspended cylinders. The effect of an adjacent boundary or ocean bed on fixed and oscillating cylinders should be studied for the unbalanced pressure of accelerating flow. Erodible and fixed bed boundaries should be included, with attempts made to measure velocity changes between the cylinder and boundary and to measure changes of boundary shape.

SCOUR

Possible scour on the ocean bottom near the Aqueduct is the least known factor of all, especially when considering extreme century risks. Ocean bed sediment transport, as computed by a theoretical-mathematical type model, has not been verified by field observations. Sediment transport computations and modeling theory exist only for noncohesive

sand sediments, and not for the cohesive fine particle or clay type sediments. Better information about scour conditions can be obtained by model and onsite tests and observation of the ocean bed around objects near and on the ocean bed. Although model studies are convenient for varying different parameters and to simulate rare events, they need to be verified with actual data. Onsite data are always required so that sediment models can be verified as to reproducing some historical event or made to do so. Effort should be made to determine adequate modeling techniques and scaling for cohesive soils. Achieving this would be considered a technological breakthrough.

Model tests would help determine scour tendencies for various pipeline concepts such as buoyant pipelines above the bed and pipelines resting or partially buried in the ocean bed. Water flowing around a large pipeline causes local flow acceleration. Scour tendency is increased by this acceleration, even if the pipeline is somewhat above the ocean bottom, such as for the buoyant concept. Model tests would also be valuable in studying and learning more about the interdependent relationship between scour and the acceleration flow field of large diameter pipe sections and other shaped objects on or near the ocean floor.

Onsite tests should be made with different structural shapes which are of interest. Structures representing anchor blocks should

be set at various locations on the ocean bottom, from deep water up to the surf zone, and on different types of marine soils. Observations and measurements should be made in an effort to obtain correlations between scour, settlement, water depth, wave parameters, anchor block size and shape, and soil properties.

MARINE FOULING

For the buoyant concept, marine fouling can be a serious problem. Weight of the marine growth may exceed buoyant uplift on the pipeline. Such problems as the rate at which marine growth weight accrues, weight with respect to water depth and time, and possible methods of controlling or removing the growth need studying.

BOTTOM OCEAN CURRENTS

Bottom currents are the greatest threat to the California Undersea Aqueduct. Sufficient basic data concerning effects of internal wave, upwelling, and wave orbit surge components and variance of geodetic flows are lacking. Thorough oceanographic survey programs for obtaining detailed current data along proposed pipe alinements must necessarily be conducted prior to final design and construction.

REFERENCES CITED

1. Riffenburgh, R. H., January 1973, California Undersea Aqueduct Reconnaissance: The Oceanography (CUARO), Marine Environment Division, NUC-TP-353, San Diego, California, prepared for USBR.

2. U.S. Bureau of Reclamation, December 1972, California Undersea Aqueduct, Hydrodynamic loading and scour, Data and Reference Book: Draft on file at USBR Engineering and Research Center, Denver, Colorado, Unpublished.

3. _____, September 1971, Working Document, Study Work Plan, California Undersea Aqueduct, Reconnaissance Investigation.

4. Bingham, E. C., 1922, Fluidity and Plasticity, McGraw-Hill.

5. Einstein, H. A., 1970, A Literature Review on Erosion and Deposition of Sediment Near Structures in the Ocean.

6. Anonymous, March 1966, ASCE Preliminary Research on Pipeline Flotation, Report of the Pipeline Flotation Research Council and R. A. Rait, Journal of Pipeline Division, Vol. 92, PLI, p. 71.

7. Demars, K. R., and Anderson, D. G., October 1970, Environmental Factors Affecting the Emplacement of Seafloor Installation: Naval Facilities Engineering Command, 84 pages.

8. Einstein, H. A., and Wiegel, R. L., February 1970, A Literature Review on Erosion and Deposition of Sediment Near Structures in the Ocean, U.S. Naval Civil Engineering Laboratory, Port Hueneme, California, 183 pages.

9. Richart, F. E., Jr., Hall, J. R., Jr., and Woods, R. D., 1970, Vibrations of Soils and Foundations: Englewood Cliffs, New Jersey, Prentice-Hall, pp. 6-36.

10. Brown, R. J., September 16, 1967, Soil Mechanics Important in Marine Pipeline Construction: The Oil and Gas Journal, pp. 151-155.

11. Kreppert, E. G., and Clark, F. N., February 1969, The Possible Effects of a Proposed Undersea Aqueduct on Marine Ecology and of Marine Environment on the Aqueduct: Marine Advisors, Inc., La Jolla, California, p. 57.

12. Beckman, Herbert, and Thibodeaux, M. H., May 1962, Wave Force Measurements for Offshore Pipelines: Journal of Waterways and Harbors, ASCE, WW2, p. 125, and Discussion WW1, February 1963, p. 61.

13. Achenback, E., Influence of Surface Roughness on the Crossflow Around a Circular Cylinder, Journal Fluid Mech., Vol. 46, Part 2, pp. 321-335.

14. Wilson, J. F., and Caldwell, H. M., November 1971, Force and Stability Measurements on Models of Submerged Pipelines: American Society of Civil Engineers Transactions, Journal of Engineering for Industry, pp. 1290-1298.

15. Litton Systems, AMTD, June 13, 1969, Ocean Environment and Design Considerations in a Prereconnaissance Study of a California Undersea Aqueduct: Contract No. 14-06-D-6780.

16. Weigel, R. L., Beebe, K. E., and Moon, J., 1959, Ocean Wave Forces on Circular Cylindrical Piles: American Society of Civil Engineers Transactions, Vol. 124, pp. 89-116.

17. Kuelegan, G. H., and Carpenter, L. H., May 1958, Forces on Cylinders and Plates in an Oscillating Fluid: Research of the National Bureau of Standards, Vol. 60, No. 5, Research Paper 285, pp. 423-440.

18. Laird, A. D. K., Johnson, C. A., and Walker, R. W., March 1959, Water Forces on Accelerated Cylinders: Journal of Waterways and Harbors Division, American Society of Civil Engineers, WW1, pp. 99-119.

19. Beckmann, H., and Thibodeaux, M. H., May 1962, Wave Force Coefficients for Offshore Pipelines: Journal of Waterways and Harbors Division, American Society of Civil Engineers, WW2.

20. Laird, A. D. K., August 1962, Water Forces on Flexible Oscillating Cylinders: Journal of Waterways and Harbors Division, American Society of Civil Engineers Proceedings, Vol. 88, pp. 125-137.

21. Surry, David, 1972, Some Effects of Intense Turbulence on the Aerodynamics of a Circular Cylinder at Subcritical Reynolds Number: Journal of Fluid Mech., Vol. 52, Part 3, pp. 543-563.

22. Wilson, B. W., and Reid, R. O., February 1963, A Discussion of Wave Force Coefficients for Offshore Pipelines: American Society of Civil Engineers Proceedings, WW1, pp. 61-63.

23. Bearman, P. W., July 1969, Vortex Shedding From a Circular Cylinder, Journal of Fluid Mech., Vol. 37, Part 3, p. 584.

24. Shalak, Richard, Editor, 1964, Oceanographical Engineering, Prentice-Hall series in Fluid Mechanics.

25. Meyers, J. J., Editor, 1969, Handbook of Ocean and Underwater Engineering: McGraw-Hill Book Company.

26. Brown, R. J., March, November 1967, Hydrodynamic Forces on Submarine Pipeline: American Society of Civil Engineers, Journal of Pipeline Division, PL1, pp. 9-19, and discussions PL3, pp. 75-81.

27. Font, Juan B., November 1967, Discussion of Reference 13: Journal of Pipeline Division, American Society of Civil Engineers, PL3, pp. 77-80.

28. Chiu, W. S., and Lienhard, J. H., December 1967, On Real Fluid Flow Over Yawed Circular Cylinders: ASME, Journal of Basin Engineering, December 1967, pp. 851-857.

29. Schlichting, H., 1968, Boundary-layer Theory: New York, McGraw-Hill, 6th Edition, pp. 241-242.

30. Ippen, A. T., 1966, Estuary and Coastline Hydrodynamics: McGraw-Hill Book Company, Inc., pp. 14-20.

31. LeMehaute, D. Divoky, and Lin, A., September 1968, Shallow Water Waves, Proceedings of Eleventh Conference on Coastal Engineering: London, England, Vol. 1, pp. 86-107.

32. Handbook of Ocean and Underwater Engineering, 1969, New York, McGraw-Hill Book Company, 1969.

33. Einstein, Hans, et al., 1970, A Literature Review on Erosion and Deposition of Sediment Structures in the Ocean: University of California.

34. Gibbs, H. J., Report EM-643: U.S. Bureau of Reclamation.

35. Leliavsky, S., 1954, An Introduction to Fluvial Hydraulics: Constable and Company, Ltd.

36. Bird, Stewart, Lightfoot, 1960, Transport Phenomena, Wiley.

37. Graf, W. H., 1971, Hydraulics of Sediment Transport.

38. Lane, E. W., 1952, Progress Report on the Design of Stable Channels: Bureau of Reclamation Report, HYD 352.

39. Shields, A., 1936, Anwendung der Ahnlichkeitsmechanik and Turbulenzforschung auf die Geschiebebewegung, Mitteil: Preuss. Versuchsanst. Wasser, Erd, Schiffsbau, Berlin, no. 26.

40. Gessler, J., 1965, Der Geschiebetriebbeginn bei Mischungen untersucht an naturlichen Abpflasterungserscheinungen in Kanalen, Mitteil: VAWE, Eidgen, Techn. Hochschule, Zurich, no. 69. Translation T-5. W. M. Keck Laboratory, California Institute of Technology, Pasadena, California.

41. Naval Civil Engineering Laboratories, 1971, Environmental Factors Affecting the Emplacement of Seafloor Installation.

42. Hjulstrom, 1935, Morphological Activity of Rivers as Illustrated by River Fyris: Bulletin Geological Institute, Uppsals, Vol. 25, Chapter III.

43. Laursen, E. M., 1951, Progress Report of Model Studies of Scour Around Bridge Piers and Abutments: Research Report No. 13-B Highway Research Board.

44. Shen, H. W., et al., 1969, Local Scour Around Bridge Piers: American Society of Civil Engineers, Proceedings, Journal of the Hydraulic Division, Vol. 95, No. HY6.

45. _____, Schneider, V. R., and Karaki, S. S., 1966, Mechanics of local scour: Engineering & Research Center, Colorado State University, Report No. CER 66HWS22, Fort Collins, Colorado.

46. _____, Ogawa, Y., and Karaki, S. S., 1965, Time variation of bed deformation near bridge piers: In Proceedings, 11th Congress International Association for Hydraulic Research, Leningrad, September 7-11, 1965, Vol. 3. Moscow, Committee for the USSR Participation in International Power Conferences, 1965, paper 3.14.

47. Carstens, M. R., May 1966, Similarity laws for localized scour: American Society of Civil Engineers, Proceedings, Journal of the Hydraulics Division, Vol. 92, No. HY3, pp. 13-36.

48. Larras, J., Profendeurs Maximales d'erosion des fonds mobiles autour des piles en riviere, (Maximum Depth of Erosion in Shifting Beds Around River Piles), Vol. 133, No. 4, pp. 411-424.

49. Posey, C. J., 1971, Protection of offshore structures against underscour: American Society of Civil Engineers, Journal of the Hydraulic Division, Vol. 97, HY7, pp. 1011-1015.

50. Trask, P. D., Movement of sand around southern California promontories: U.S. Army Beach Erosion Board TM No. 76.

SOURCES OF DATA CONTACTED

During the course of collecting and evaluating the data for the NUC contract work, many institutes and individuals were contacted by NUC. The list of these sources from NUC Technical Paper No. 353[1] is reproduced here.

INSTITUTIONAL SOURCES OF ARCHIVED DATA

American Geophysical Union
Army Corps of Engineers
    Beach Erosion Board
    Navigation and Shoreline Planning Branch
Association of Monterey Bay Area Governments
Bodega Marine Laboratory
California Academy of Science, Steinhart Aquarium
California Institute of Technology
California Research Corporation
California State University, San Diego
Crescent City
Coastal Engineers Research Center
Coast and Geodetic Survey
Department of Fish and Game, State of California
Engineering Foundation
Engineering Science, Inc.
Environmental Protection Agency
Environmental Prediction Research Facility, U. S. Navy
Environmental Science Service Foundation, Department of Commerce
Esso Oil Corporation
Fleet Numerical Weather Central, Monterey, U. S. Navy
Hopkins Marine Station, Stanford University
Humble Oil Corporation
Humboldt State College
Intersea Research Corporation
Marine Resources Laboratory, Marine Technology Center, State of California
    Menlo Park Laboratory
    Monterey Laboratory
Moss Landing Marine Laboratory
National Academy of Science
National Bureau of Standards
National Marine Fisheries Service
    La Jolla
    Monterey
    Tiburon
National Marine Consultants
National Marine Minerals Technology Center
National Oceanographic Data Center, NOAA
National Ocean Survey, NOAA
National Research Council
Naval Civil Engineering Laboratory
Naval Postgraduate School
Naval Supply Center
Naval Undersea Center

Office of Naval Research, General Oceanography Support
Oregon State University
Pacific Gas and Electric Co., Inc.
Pacific Marine Station, Dillon Beach
Plessey Environmental Systems
San Diego Marine Consultants
San Francisco Bar Pilots Association
Southern California Coastal Water Resources Project
Stanford University, Department of Geology
State Department of Navigation and Ocean Development (California)
State Division of Mines and Geology, Department of Conservation (California)
State Water Quality Control Board (California)
    Los Angeles
    Sacramento
    San Diego
Tetra-Tech, Inc.
University of California, Berkeley
    College of Engineering
    Hydraulics Engineering Laboratory
    Water Resources Center Archives
University of California, Los Angeles
University of California, Santa Cruz
University of California, San Diego
    Institute for Geophysics and Planetary Physics
    Scripps Institution of Oceanography
University of Southern California, Hancock Foundation
United States Coast Guard, San Diego
United States Geological Survey
    National Center for Earthquake Research
    Office of Marine Geology and Hydrology
Westinghouse Ocean Research Laboratory

INDIVIDUALS AS SOURCES OF DATA

Anderson, Dr. Victor, MPL, SIO, UCSD, Ca.
Arnel, Dr. Robert, Director, Moss Landing Marine Laboratory, Moss Landing, Ca.
Austin Roz, Visibility Laboratory, MPL, SIO, UCSD, Ca.
Bakun, Andrew, NMFS, Monterey, Ca.
Baldridge, Allan, Hopkins Marine Station, Stanford University, Pacific Grove, Ca.
Barakos, Dr. Peter, Marine Environment Division, NUC, San Diego, Ca.
Beeman, Dr. Robert, Department of Marine Biology, San Francisco State College, San Francisco, Ca.
Bell, Robert, Department of Fish and Game, State of California, Long Beach, Ca.
Bissell, Harold, Department of Water Resources, State of California, Sacramento, Ca.
Boden, Dr. Bette, Marine Biology Research Division, SIO, UCSD, Ca.
Broenkow, Dr. Walter, Moss Landing Marine Laboratory, Moss Landing, Ca.
Brown, Daniel, MLRG, SIO, UCSD, Ca.
Brown, Robert, Plessey Environmental Systems, San Diego, Ca.
Cairns, James, IGPP, UCSD, on leave from Marine Environment Division, NUC, San Diego, Ca.
Carlson, P. R., USGS, Menlo Park, Ca.
Carsola, Dr. Al, SCCWRP, Los Angeles, Ca.
Chase, Thomas, GRD, SIO, UCSD, Ca.
Church, Dr. Ron, Environmental Protection Agency, Washington, D. C.
Clark, William, Westinghouse Ocean Research Laboratory, Annapolis, Md.
Conomos, John, USGS, Menlo Park, Ca.
Corliss, Roy E., Coastal Pollution Program, Naval Supply Center, Oakland, Ca.
Costello, James, MLRG, SIO, UCSD, Ca.
Cotton, William, USGS, Menlo Park, Ca.
Cox, Dr. Charles, Department SIO, UCSD, Ca.
Crandall, Dr., Department of Oceanography, Humboldt State College, Arcata, Ca.
Davoll, Peter, Hopkins Marine Station, Stanford University, Pacific Grove, Ca.
Dill, Dr. Robert F., NOAA, Washington, D. C.
Doyle, James, Engineering Research Division, Pacific Gas and Electric Co., Emeryville, Ca.
Drake, Dr. David, Hancock Foundation, USC, Los Angeles, Ca.
Eaton, Dr. Jerry, Director, National Center for Earthquake Research, Menlo Park, Ca.
Fager, Dr. William, Department SIO, CSUSD, Ca.
Ferris, David, Department of Biology, CSUSD, Ca.
Flittner, Dr. Glenn, Director, Office of Marine Research, CSUSD, Ca.
Forsberg, Eric, NMFS, La Jolla, Ca.
Fox, Dean, Simonson Logging Co. (diver), Crescent City, Ca.
Gast, Dr. James, Department of Oceanography, Humboldt State College, Arcata, Ca.
Gorsline, Dr. Donald, Hancock Foundation, USC, Los Angeles, Ca.
Gotshall, David, Marine Resources Agency, MTC, State of California, Monterey, Ca.
Griggs, Dr. Gary, Department of Geology, University of California, Santa Cruz, Ca.
Hamilton, CDR Glen (Ph. D.), EPRF, Monterey, Ca.
Hand, Dr. Cadet, Director, Bodega Marine Laboratory, Bodega Bay, Ca.
Harrison, CDR Avery, United States Coast Guard, San Diego, Ca.
Hedgpeth, Dr. Joel, Pacific Marine Station, Dillon Beach, Ca.

Ingle, Dr. James, Department of Geology, Stanford University, Stanford, Ca.
Inman, Dr. Douglas, ORD, SIO, UCSD, Ca.
Isaacs, Prof. John, MLRG, SIO, UCSD, Ca.
Johnson, James H., NMFS, Monterey, Ca.
Johnson, Dr. J. W., Hydraulics Laboratory, UCB, Ca.
Kolpack, Dr. Ronald, Hancock Foundation, USC, Los Angeles, Ca.
Kor, Benjamin, State Water Quality Control Board, Sacramento, Ca.
Laevastu, Dr. Taivo, EPRF, Monterey, Ca.
LaFond, Dr. Eugene, Consultant for Oceanography, NUC, San Diego, Ca.
Laurs, Dr. Michael, NMFS, La Jolla, Ca.
Lazanoff, Shelley, Naval Oceanographic Office, Monterey, Ca.
Lee, Dr., Hopkins Marine Station, Stanford University, Pacific Grove, Ca.
Lee, Sara, CalCOFI, La Jolla, Ca.
Leiper, Dr. Dale, Chairman, Department of Oceanography, NPGS, Monterey, Ca.
Le Méhauté, Dr., Tetra-Tech, Inc., Pasadena, Ca.
Lewitt, LCDR Howard, Fleet Numerical Weather Facility, Monterey, Ca.
Lynn, Ronald, NMFS, La Jolla, Ca.
Mallett, Linford, diver, Crescent City, Ca.
Marshall, Neil, ORD, SIO, UCSD, Ca.
McAlister, Ed, MPL, SIO, UCSD, Ca.
McLain, Dr. Douglas, NMFS, Monterey, Ca.
Mudie, Dr. John, MPL, SIO, UCSD, Ca.
Munk, Dr. Walter, Director, IGPP, UCSD, Ca.
Nelson, Arthur P., Director, Marine Minerals Technology Center, NOAA, Tiberon, Ca.
Noda, Ed, Tetra-Tech, Inc., Pasadena, Ca.
Nordstrom, Charles, ORD, SIO, UCSD, Ca.
North, Dr. Wheeler J., Environmental Studies Program, California Institute of Technology, Pasadena, Ca.
O'Leary, Dennis, State Water Quality Control Board, San Diego, Ca.
Olson, Jack, Marine Environment Division, NUC, San Diego, Ca.
Orcutt, Dr. Harold, Marine Research Laboratory, MTC, Menlo Park, Ca.
Paquette, Dr. Robert, NPGS, Monterey, Ca.
Pequegnat, Dr., Department of Oceanography, Humboldt State College, Arcata, Ca.
Pestrong, Raymond, Chairman, Department of Geology, San Francisco State College, San Francisco, Ca.
Petrie, William L., National Academy of Sciences, Washington, D. C.
Rabe, Kevin, EPRF, Monterey, Ca.
Reid, Joseph, Department SIO, UCSD, Ca.
Richerček, Darold G., Harbor Master, Crescent City, Ca.
Robinson, Margaret, ORD, SIO, UCSD, Ca.
Schafran, Walter C., Fisheries Program, Humboldt State College, Arcata, Ca.
Schwartzlose, Dr. Richard P., MLRG, SIO, UCSD, Ca.
Seckel, Gunther R., NMFS, Monterey, Ca.
Shepard, Dr. Francis P., Professor Emeritus, GRD, SIO, UCSD, Ca.
Silver, Ely, USGS, Menlo Park, Ca.
Simons, Richard, IGPP, UCSD, Ca.